CANADIAN THESES

THÈSES CANADIENNES

NOTICE

The quality of this microfiche is heavily dependent upon the quality of the original thesis submitted for microfilming. Every effort has been made to ensure the highest quality of reproduction possible.

If pages are missing, contact the university which granted the degree.

Some pages may have indistinct print especially if the original pages were typed with a poor typewriter ribbon or if the university sent us an inferior photocopy.

Previously copyrighted materials (journal articles, published tests, etc.) are not filmed.

Reproduction in full or in part of this film is governed by the Canadian Copyright Act, R.S.C. 1970, c. C-30.

AVIS

La qualité de cette microfiche dépend grandement de la qualité de la thèse soumise au microfilmage. Nous avons tout fait pour assurer une qualité supérieure de reproduction.

S'il manque des pages, veuillez communiquer avec l'université qui a conféré le grade.

La qualité d'impression de certaines pages peut laisser à désirer, surtout si les pages originales ont été dactylographiées à l'aide d'un ruban usé ou si l'université nous a fait parvenir une photocopie de qualité inférieure.

Les documents qui font déjà l'objet d'un droit d'auteur (articles de revue, examens publiés, etc.) ne sont pas microfilmés.

La reproduction, même partielle, de ce microfilm est soumise à la Loi canadienne sur le droit d'auteur, SRC 1970, c. C-30.

THIS DISSERTATION
HAS BEEN MICROFILMED
EXACTLY AS RECEIVED

LA THÈSE A ÉTÉ
MICROFILMÉE TELLE QUE
NOUS L'AVONS REÇUE

THE EXCHANGE INTERACTION AND SINGLE CRYSTAL GROWTH OF SELECTED SEMIMAGNETIC SEMICONDUCTORS

by

Douglas J.S. Beckett

Thesis submitted to the
School of Graduate Studies
in partial fulfillment of the requirements
for the degree of
Master of Science in Physics

Department of Physics
Faculty of Science
University of Ottawa
Ottawa, Canada

ISBN 0-315-36469-6

UNIVERSITÉ D'OTTAWA
UNIVERSITY OF OTTAWA

ABSTRACT

Two subjects contributing to the understanding of semimagnetic semiconductors are presented in this thesis.

The first subject is that of single crystal growth of the pseudo-ternary semimagnetic semiconductor alloy $Cd_xZn_yMn_zTe$ $(x + y + z = 1)$. Comparisons are made between single crystals, grown by the Bridgman method, and polycrystal grown by the melt and anneal technique. Results of this comparison indicate a small separation of the liquidus and solidus surfaces in the temperature-composition ternary phase diagram. Also important is the lack of any observable difference in the magnetic properties of single crystals and polycrystals.

The second topic deals with the exchange interaction in the pseudo-ternary semimagnetic semiconductor $Cd_xHg_yMn_zTe$ $(x + y + z = 1)$ alloy. Results of X-ray, magnetic susceptibility and optical energy gap measurements reveal a significant enhancement of the Mn-Mn exchange energy for low band-gap, due to virtual interband transitions. This increase in energy is analysed according to the theories of Bloembergen and Rowland, and Abrikosov, and is found to have qualitative agreement with both. Experimental error, however, prevents definitive conclusions from being drawn.

ACKNOWLEDGEMENTS

First, I would like to thank Dr. J.C. Woolley for his advice and encouragement during the research on CdHgMnTe and the writing of this thesis.

Thanks are also due to Dr. P. Bernard for his contributions in building the Bridgman furnace, and for providing advice and assistance in the growth of single crystals.

I would also like to thank Dr. G. Lamarche for the use of his magnetic susceptibility apparatus, and for his patient explanations of that apparatus and many other subjects.

I would like to thank Mr. Sudershan Manhas for providing some samples of CdHgMnTe, and to Dr. Tom Donofrio for providing data on CdZnMnTe, as well as his excellent diagram of the magnetic susceptibility apparatus.

I wish to express my appreciation to Mr. Robert Hart and the other technicians of the machine shop for constructing the Bridgman furnace and countless other items, and for seeming to have completed jobs before they were even submitted.

I owe innumerable thanks to my mother-in-law, Mrs. Lise Dionne, for her tireless typing, and for saving me from endless hours at the keyboard.

Most of all, I would like to thank my wife, Michèle, for her support, both emotional and financial, during the trials of the last two years.

TABLE OF CONTENTS

LIST OF FIGURES

LIST OF TABLES

INTRODUCTION

1.1 Background

In recent years, there has been a great amount of interest in the subject of semimagnetic semiconductors (SMSC's) (84B1, 82G1). These are materials in which an ordinary semiconductor has been alloyed with a magnetic semiconductor. The introduction of a magnetic component to a semiconductor lattice results in many interesting properties.

These properties include large magneto-optical effects, magnetic field dependence of acceptor activation energy, g-factor enhancement, and solely magnetic properties, such as spin glass behaviour (84B1).

Almost all of the SMSC's studied are II-VI compounds alloyed with a transition metal compound, forming a pseudo-binary alloy. The predominant alloys are $Cd_{1-z}Mn_zTe$ and $Hg_{1-z}Mn_zTe$. Other examples are $Sn_{1-z}Mn_zTe$, $Cd_{1-z}Mn_zSe$, $Zn_{1-z}Mn_zTe$, $Pb_{1-z}Fe_zTe$ etc. There are many other possible pseudo-binary alloy combinations.

The interest in these materials can be attributed to two factors: the many fascinating observations with corresponding theoretical explanations; and the fertile ground for further study provided by the multitude of properties which can be varied by changing alloy compositions or components.

The research described in this thesis was performed in the semiconductor laboratory at the University of Ottawa, where investigation of SMSC's has been extended to include pseudo-ternary alloys, such as $Cd_xZn_yMn_zTe$ ($x + y + z = 1$). This approach allows for two independent variables so that, for example an alloy with a specific manganese concentration and energy gap can be made.

1.2 Single Crystal Growth

Until this present work, all of the SHSC alloys made at the University of Ottawa had been polycrystalline samples made by the melt and anneal technique. The reason for this is that the pseudo-ternary alloys being studied had not been investigated previously. As a result, initial crystallographic work had to be performed in addition to the other experiments. For crystallographic work, homogeneous polycrystalline samples are necessary. They allow for simple identification of the limits of solid solution in the alloy, while avoiding the complications of composition gradients which are most often present in single crystals.

Another advantage of polycrystalline specimens is the ease, relative to single crystal samples, with which they are made. A student can easily prepare and melt twenty-five samples in one week, with the annealing time being typically one month. Also, this process requires only relatively inexpensive temperature controllers and wire-wound furnaces. This method is also easily learned and safe.

The growth of single crystals requires much larger investments in time and money. In the absence of ~~(expensive)~~ full time technical assistance, the time required to master the desired growth technique is usually prohibitive for a graduate student looking to finish his or her degree in a reasonable time.

The reasons why most researchers grow single crystals is that, the initial crystallographic work having been done, they wish to perform electrical and optical measurements requiring a low amount of defects. Crystal orientation is also a factor for some experiments, such as Raman scattering (84B1).

As was the case for the initial work on pseudo-binary alloys, single crystals were considered unnecessary for the measurements performed at the University of Ottawa. These measurements include magnetic susceptibility, optical energy gap and electron spin resonance. However, to extend the measurements on the pseudo-ternary alloys to electrical properties and more sophisticated optical properties, single crystal specimens are required.

Another important consideration is that many other researchers use single crystals in their study of SMSC's. Although they work with pseudo-binary alloys, their materials often form the edges of the pseudo-ternary alloy systems grown at the University of Ottawa.

Comparisons are often made between the results obtained using polycrystalline specimens and those obtained using single crystal specimens. Thus it becomes important to know if the measurements are independent of the crystal condition.

For this reason it was decided to build an apparatus to grow single crystals by the Bridgman technique. The details of the construction of the apparatus and the growth results are given in Chapter 2 of this thesis.

The growth of single crystals is essentially a technical problem. However, it is original work in that it has not been previously investigated for most pseudo-ternary systems. It also promises to add to the knowledge about the phase diagram of the alloy system, enable research to be extended to electrical and optical properties, and allow for comparison of single crystal and polycrystalline results.

1.3 Magnetic properties of the $Cd_xHg_yMn_zTe$ alloy ($x + y + z = 1$)

The major portion of the work performed for this thesis was devoted to the study of the magnetic properties of the pseudo-ternary alloy $Cd_xHg_yMn_zTe$ ($x + y + z = 1$). The interest in this alloy stems from the fact that the energy gap goes to zero near the mercury telluride corner of the ternary diagram (Figure 1.1)(81D1). This has interesting consequences for the magnetic properties of the alloy system (84M1).

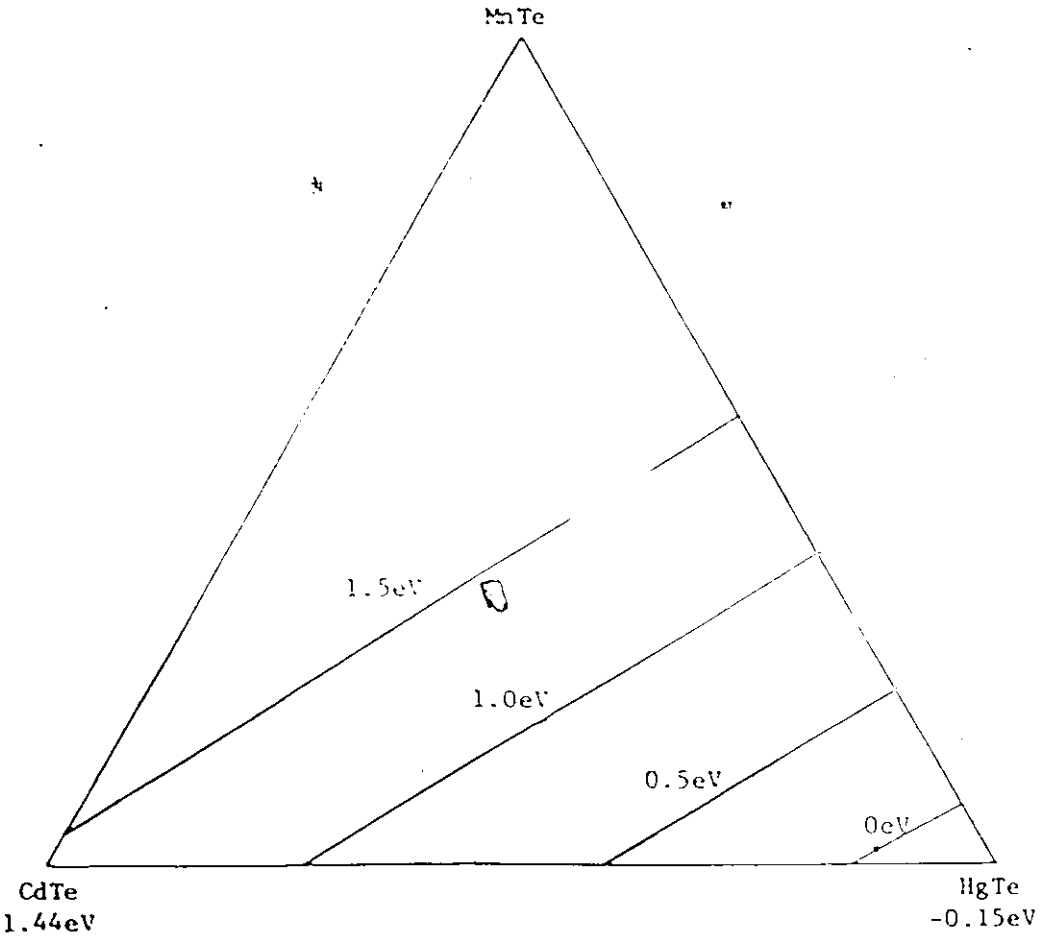

Figure 1.1 The $Cd_xHg_yMn_zTe$ pseudo-ternary diagram showing approximate lines of constant energy gap from Debska et al. (81D1).

In a wide gap SMSC, the magnetic interaction between the manganese cations has been attributed to super exchange involving virtual transitions from the valence band to the manganese $3d^6$ level (77Gl, 85Ll, 86Sl).

The important parameters in this interaction are the manganese concentration, z, and the lattice parameter. Together these determine the average distance between manganese ions.

In CdHgMnTe however, the proximity of the conduction band allows virtual transitions between the valence band and conduction band to become important. This in turn allows another form of super exchange to become significant (84Ml). This form is called the Bloembergen-Rowland interaction, and in addition to depending on the manganese concentration and lattice parameter, will depend on the energy gap.

It is the investigation of this interaction which is detailed in Chapter 3 of this thesis.

SINGLE CRYSTAL GROWTH

2.1 Introduction

Having decided to attempt to grow single crystals, one must then decide which technique is to be used. The equipment immediately available was suitable for either chemical (halogen) vapour transport or the Bridgman method, both of which are widely used methods of single crystal growth.

While annealing samples of CdZnMnTe, it was observed that in two instances the alloy partially transported and deposited itself in other parts of the quartz tube from where the bulk of the material was located. Powder X-ray pictures of the transported material were identical to those of the bulk material, indicating that they were of the same composition. This observation seemed to show that vapour transport was a promising technique for this alloy system.

In reviewing papers by other researchers in the field of SMSC's, however, it was found that the Bridgman technique is used almost exclusively for growing bulk single crystals. Other factors which went against vapour transport were the need for a glass blower to seal the larger quartz tubes used with this method, and the safety precautions required when using large tubes containing iodine vapour at high temperature.

2.2 The Bridgman Growth Technique

In order to grow single crystals of antimony, bismuth, tellurium, cadmium, zinc and tin, P.W. Bridgman developed a technique utilising a furnace with two distinct regions of different temperature

(25B1). For compounds and elements, the temperatures are chosen such that the hotter region is above the melting point of the substance being grown, while the cooler is below that melting point. The furnace is arranged vertically, and then the substance is slowly lowered from the hot region, where it is molten, into the colder region.

As it passes through the position of its melting point, the substance successively freezes. The sample holder is tapered to a point on the bottom, so that the first portion to freeze, called the "seed", is very small and will be of one crystallographic orientation. The next layers will then freeze into this first portion in the same orientation. The result is a sample having a single orientation, i.e. a single crystal.

When attempting to grow alloys, as opposed to elements and congruently melting compounds, some parameters of the alloy and the furnace become very important (73B1). Among these are: the phase diagram of the alloy; the temperature gradient of the furnace at the position of the melting point; the lowering speed of the sample; and vibration.

Since attempts to grow single crystals are only made for single phase regions of the phase diagram, it is important that there is some knowledge of the range of solid solubility. Another factor which depends on the phase diagram is the temperature separation of the liquidus and solidus. As shown in the example of Figure 2.1, the composition of the crystal being formed is quite different than the nominal composition of the melt. This in turn changes the composition of the melt with growth, resulting in a varying composition along the growth axis.

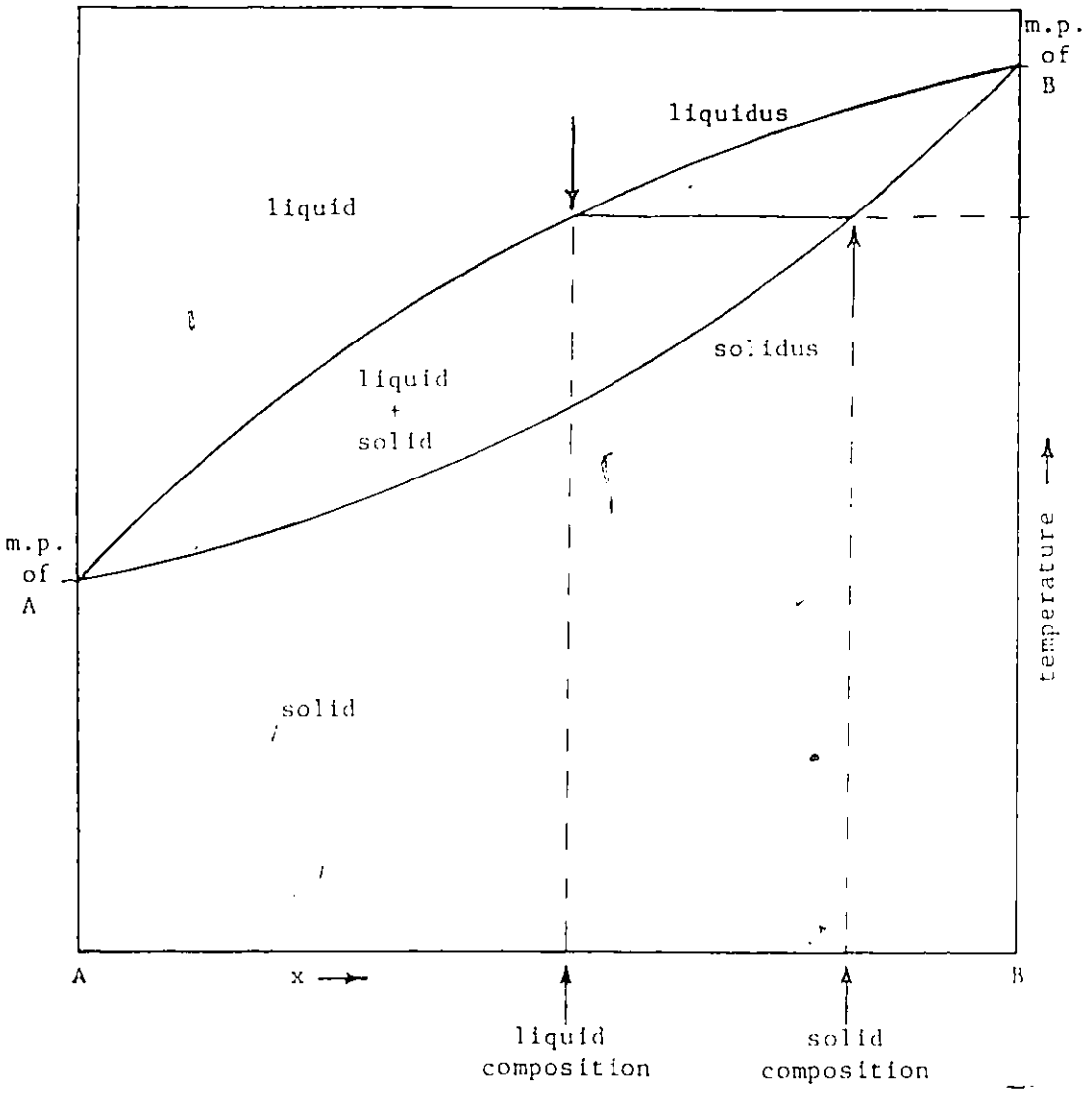

Figure 2.1 Simple temperature composition phase diagram for a binary alloy $A_{1-x}B_x$ showing the difference in composition between the liquid and the solid.

This difference in composition between the solid and liquid always occurs, but the magnitude of the difference depends on the separation of the liquidus and solidus.

In addition to causing a composition gradient, changes in the composition at the solid-liquid interface can also be an actual impediment to the growth of single crystals. A high viscosity and a fast growth rate can combine to keep a high composition gradient in the melt. If in addition to this the temperature gradient is too small, the situation can occur where the melt becomes supercooled away from the growth surface, as shown in figure 2.2. This is called constitutional supercooling. In this case there will be pieces of random orientation suddenly freezing onto the growth face, destroying the single crystal nature of the sample. To counteract this, the temperature gradient must be made as high as possible. Also the speed at which the sample is lowered can be reduced to allow the melt to become more homogeneous, by allowing more diffusion in the liquid region.

Vibration can be a problem in that it can disturb the growth orientation, but it can also aid in mixing the molten portion of the ingot.

2.3 Furnace Construction

The first five attempts at growing single crystals by the Bridgman method were made by using a furnace originally constructed for horizontal step freezing of pseudo-binary alloys. It contained two seperately heated tubes, with a water cooled copper baffle between them. These were contained in an aluminium and asbestos box,

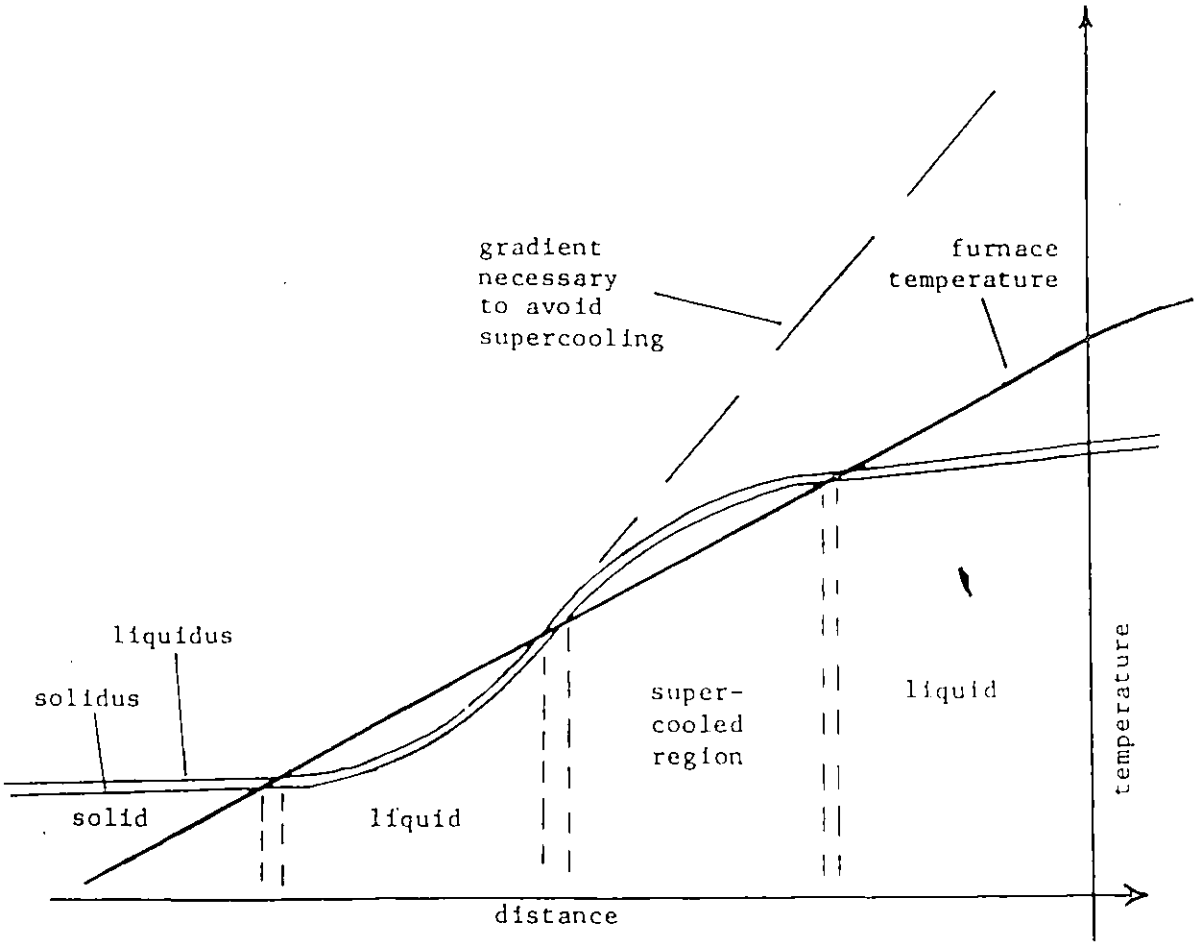

Figure 2.2 Diagram depicting constitutional supercooling of portions of the melt due to an inhomogeneous liquid and an insufficient temperature gradient.

with vermiculite as insulation. For use in the Bridgman configuration, the furnace was mounted on a wall with the axis of the tubes arranged vertically.

The temperature profile of this furnace was measured with a platinum-platinum 13% rhodium thermocouple in a long ceramic rod (120 cm.). It was found at this point that convection had a very strong impact on the temperature inside the furnace. To avoid convection, the bottom of the furnace was plugged with a bung made of firebrick.

An example of the temperature profile of the furnace as it was used for crystal growth is given in Figure 2.3. A very good temperature gradient exists, but the temperature at which this gradient occured was limited by the water cooled baffle at a depth of about 35 cm below the top. The temperatures shown in Figure 2.3 are the maximum which could be attained without the risk of immediately burning out the heating coil.

This furnace lasted long enough to grow five samples. The results of this growth are given in the next section (section 2.4). After five runs, one of the heating coils burned out. This came as no surprise, as the furnace was originally built for temperatures of around 800°C, not the 1100°C used in this case.

For this reason, and in an attempt to obtain better results, a new furnace was constructed. The details of its design are given in Figure 2.4. It is also a two-zone furnace. Fibrefrax™ insulation was found to perform very well. Fibreboard ™, which formed the outer walls, was found to be easy to work with, although it be-

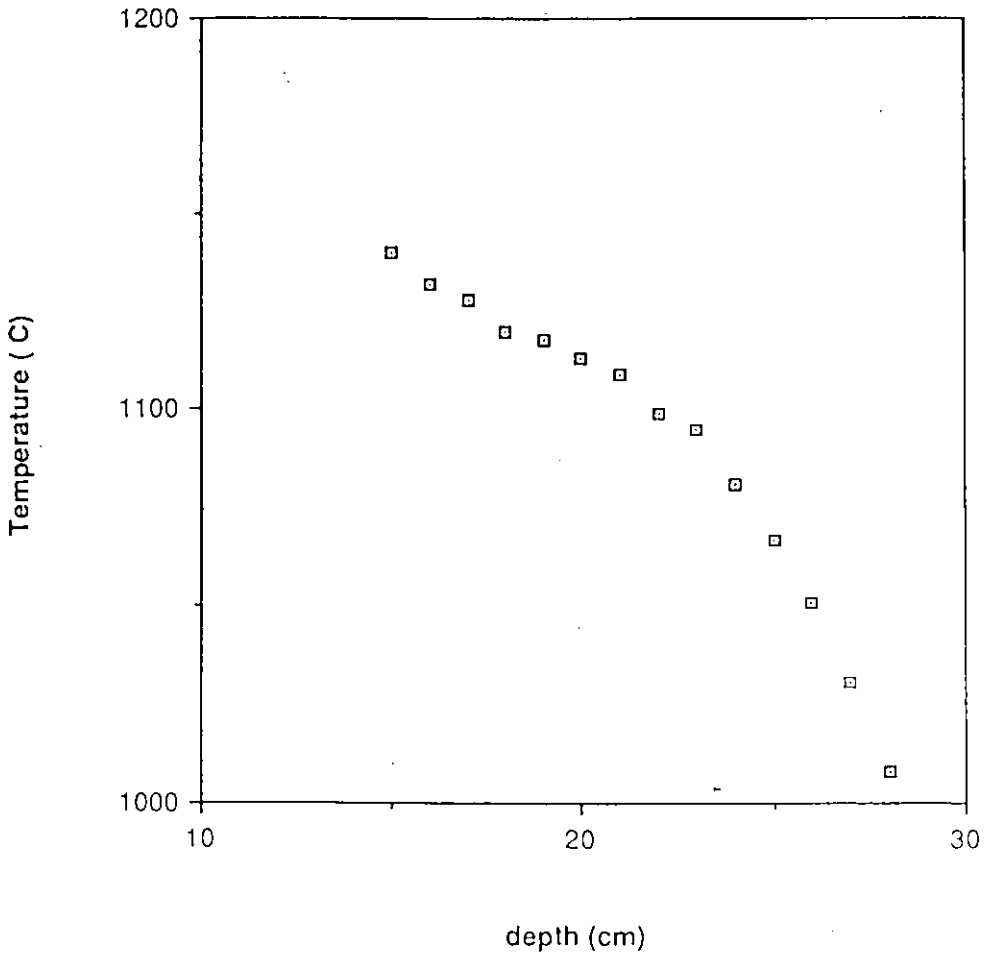

Figure 2.3 Temperature profile of the old furnace as used for crystal growth. The temperatures required for CdZnMnTe are 1050^{O}C and above.

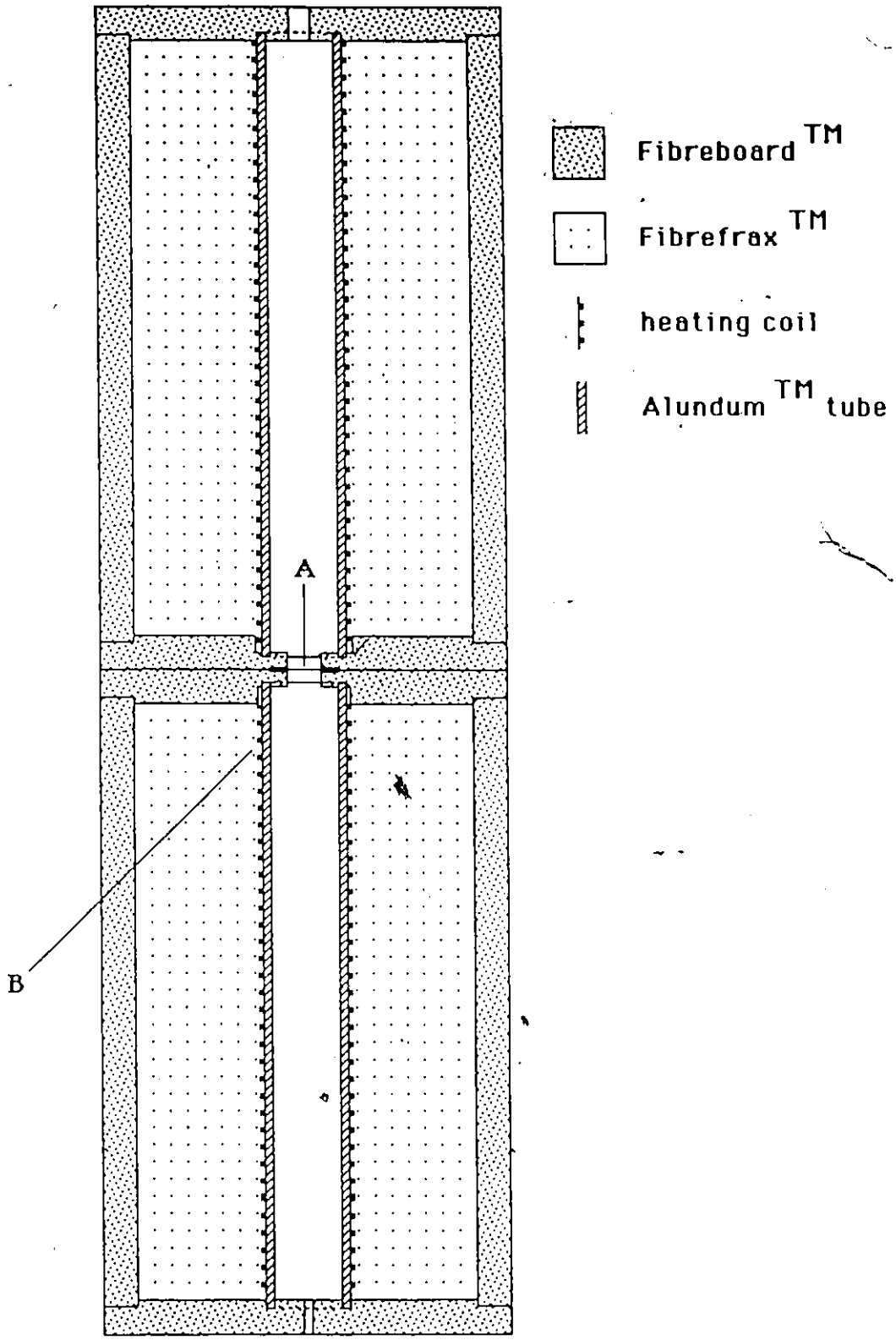

Figure 2:4 Schematic diagram of the Bridgman furnace. Arrow A shows the position of the thin platinum sheet, and arrow B, the position of a third heating coil.

came weaker after using the furnace a few times. Arrow A indicates the position of a platinum sheet (5cm x 5cm x .013cm) intended to reflect heat. Arrow B indicates the position of a third heating coil (a later addition) wound onto a new bottom tube. These measures are both designed to increase the temperature gradient at the furnace junction.

A diagram of the sample holder used with the new furnace is given in Figure 2.5. The sample holder was lowered through the furnace by a large ceramic thermocouple rod connected to a steel rod, which in turn was connected to a string. The string was slowly unwound from a spool by an electric motor whose speed was reduced by a 2500:1 transmission. The lowering speed could be varied by using spools of different diameter.

Characterisation of the furnace was again performed using the very long thermocouple. A sample plot of temperature versus depth is given in figure 2.6 for the new furnace.

2.4 Crystal Growth

Crystals of various compositions were grown using both of the Bridgman furnaces. The temperatures of the liquidus and solidus for each composition were taken from the work of Triboulet and Didier (81T1) for CdMnTe. For the pseudo-ternary alloys, these temperatures were interpolated from the values for CdMnTe and the work of Steininger and Straus (72S1) for CdZnTe. No phase diagram could be found for ZnMnTe.

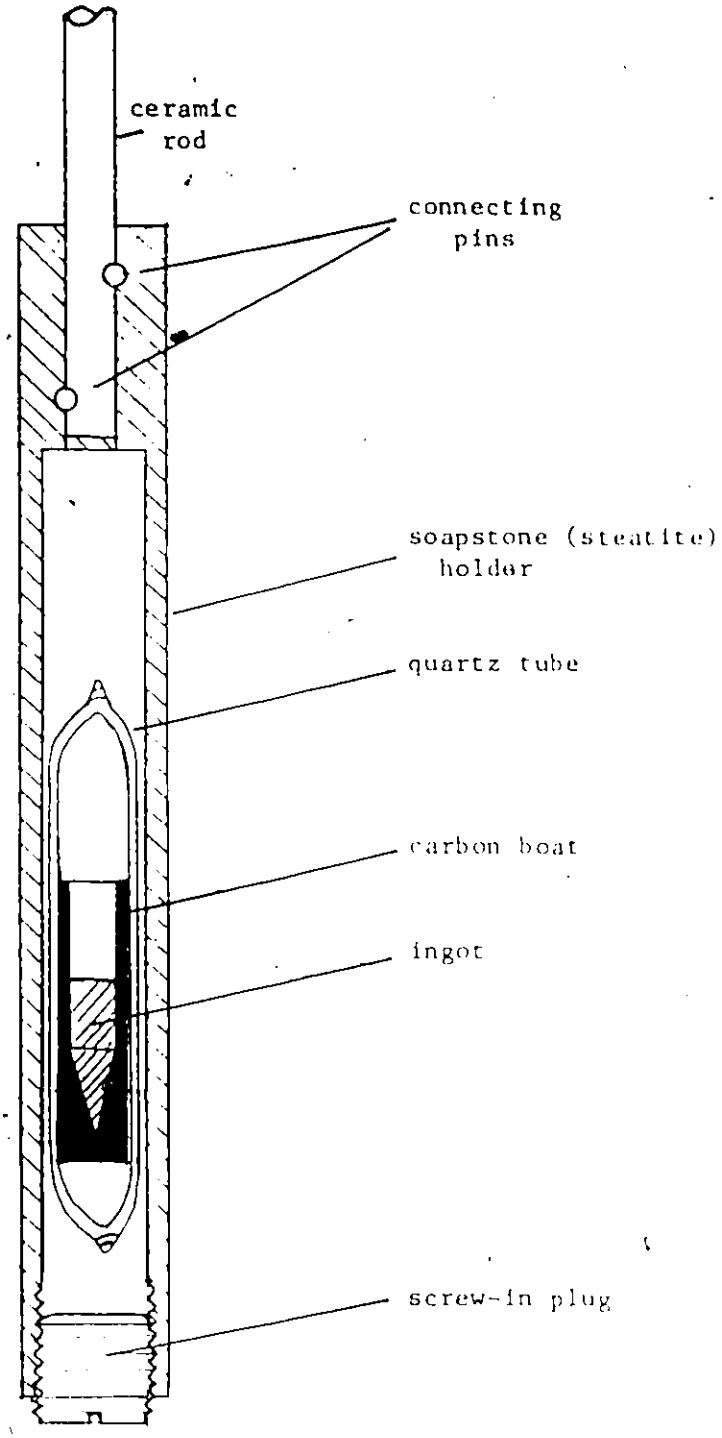

Figure 2.5 Diagram of the sample holder used for single crystal growth.

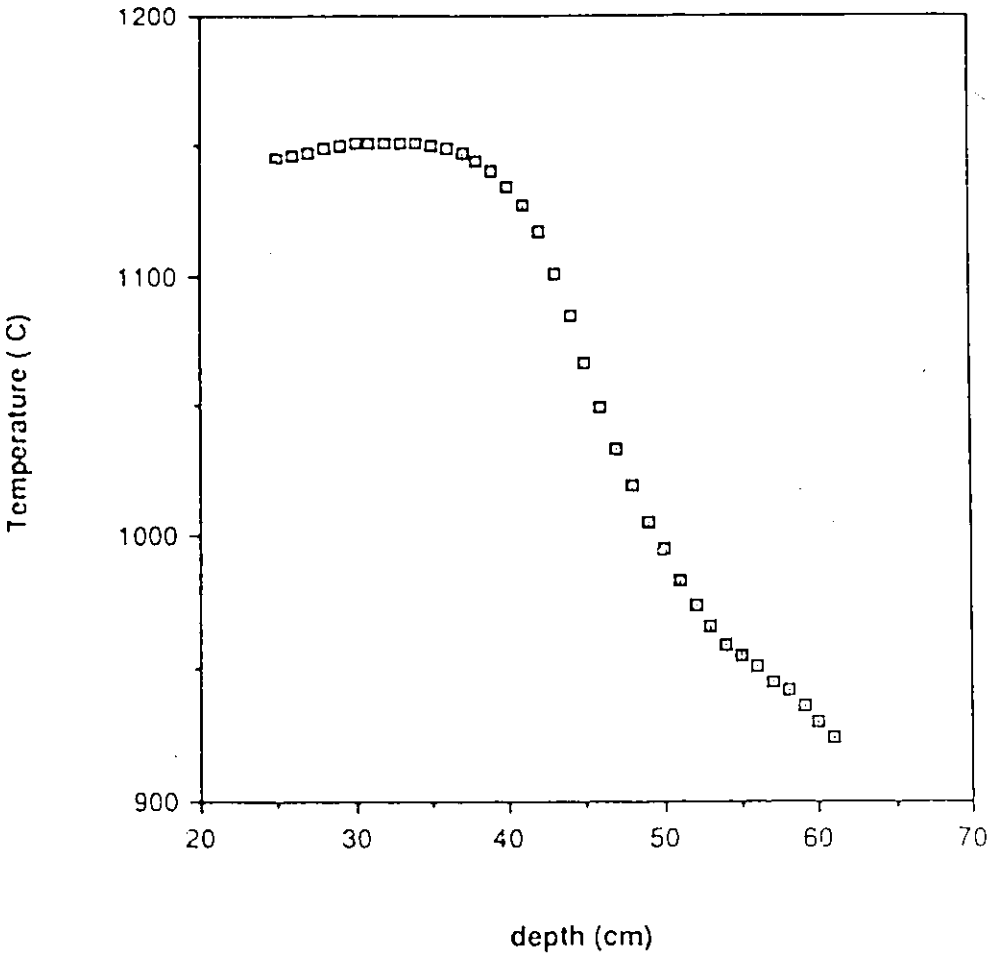

Figure 2.6 Sample plot of temperature versus depth for the Bridgman furnace.

The temperatures of the furnaces were set to be around 75°C above and below the average of the liquidus and solidus. This wide range was chosen to increase the temperature gradient at the junction (73B1), and to allow for errors in the liquidus and solidus temperatures and the temperature measurement.

The sample holder was lowered at 5 mm/hr. The first five samples were grown in the old furnace, while the next four were grown in the new one.

The limits of the single phase region for the pseudo-ternary diagram were known from the work of Brun del Re et al. (83B1).

The composition of the first sample tried (labeled BR-1) was $Cd_{.225}Zn_{.075}Mn_{.7}Te$. The result did not appear to be a single crystal. It did not cleave cleanly, and had many voids and irregularities.

A test of the nature of the crystal can be made using the method of Laue X-ray back-reflection. With this method, a beam of "white" X-rays is caused to pass through the center of a flat 10 cm x 10 cm film. The beam then strikes the crystal and is diffracted back onto the film, in a pattern which depends upon the orientation of the crystal planes. A diagram of the configuration for Laue back-reflection is given in Figure 2.7.

The resulting diffraction pattern will be a distinct set of spots for a single crystal. This pattern can be analysed so that the set of planes causing each spot is identified.

If the crystal is polycrystalline, there will be a number of such single crystal patterns superimposed. If the size of the grains

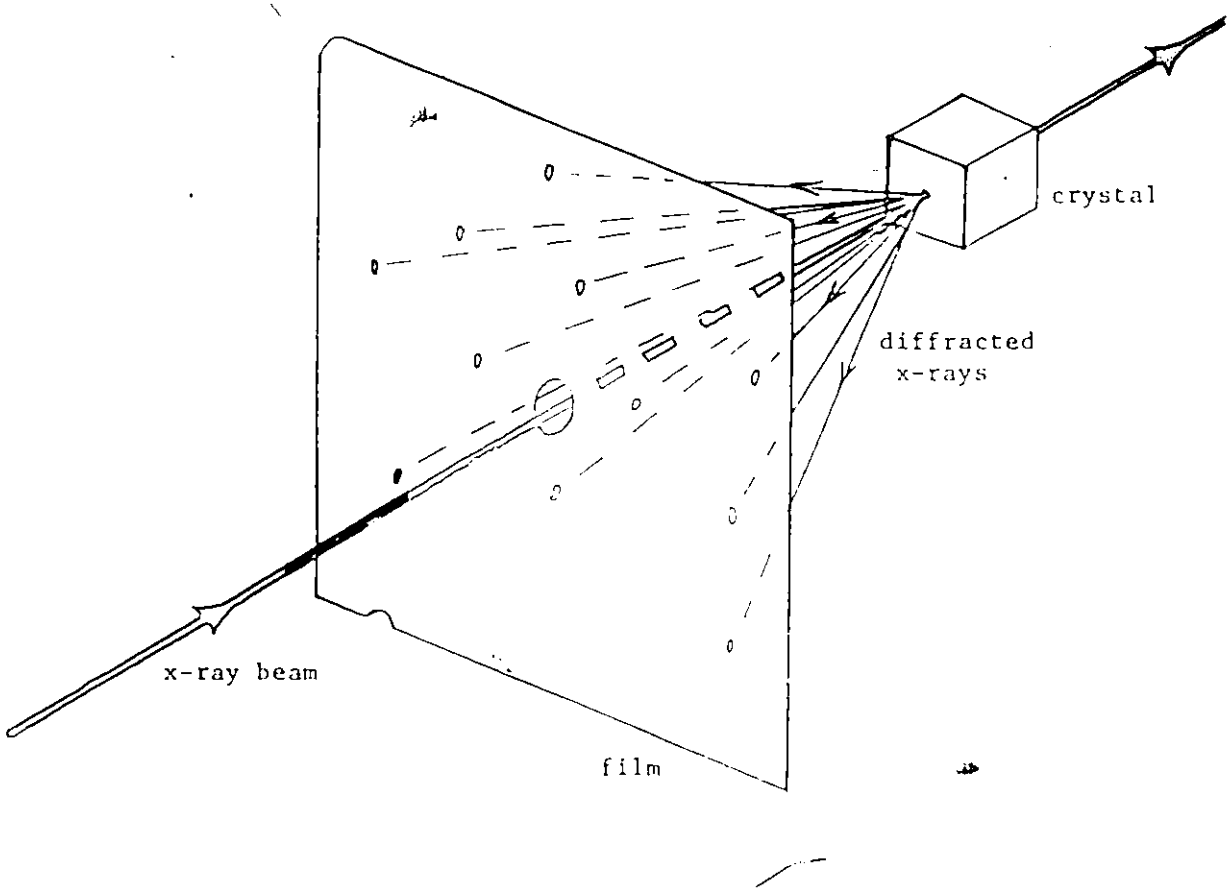

Figure 2.7 Schematic diagram of the Laue back-reflection x-ray configuration

is small enough, these patterns will be indistinguishable from the background. All that will be visible will be rings made up of diffraction spots due to the much stronger characteristic radiation of the X-ray source.

A very thorough description of the Laue method and its uses is given by Cullity (78Cl).

A small piece of sample BR-1 was analysed by the Laue method. The piece was chosen because when it was cleaved from the bulk of the ingot, it had flat faces. It was also transparent, having an orange-brown colour. The dimensions of the piece were approximately 3mm x 3mm x 1 mm.

The resulting X-ray pictures displayed patterns indicating a single crystal. The conclusion about the entire BR-1 ingot was that it was polycrystalline, but with grains as large as the X-rayed piece.

Similar results were obtained with the remaining four samples grown with the old furnace and the first one grown with the new furnace. (Samples BR-2 to BR-6). An example is given in figure 2.8 of the diffraction pattern, and in Figure 2.9 and the partially indexed stereographic projection corresponding to the pattern, for sample BR-3. The composition of BR-3 is $Cd_{.7}Mn_{.3}Te$.

Sample BR-7, grown in the new furnace, was left in the lower part of the furnace for an extra day, as it was a weekend. The result was a complete single crystal. The extra day annealing seems to have allowed one of the grains to expand at the expense of grains of other orientations. Sample BR-8 was thus left to anneal for an extra day after passing into the zone of lower temperature, and it, too,

Figure 2.8 Laue back reflection photograph of sample BR-3 showing a single crystal pattern.

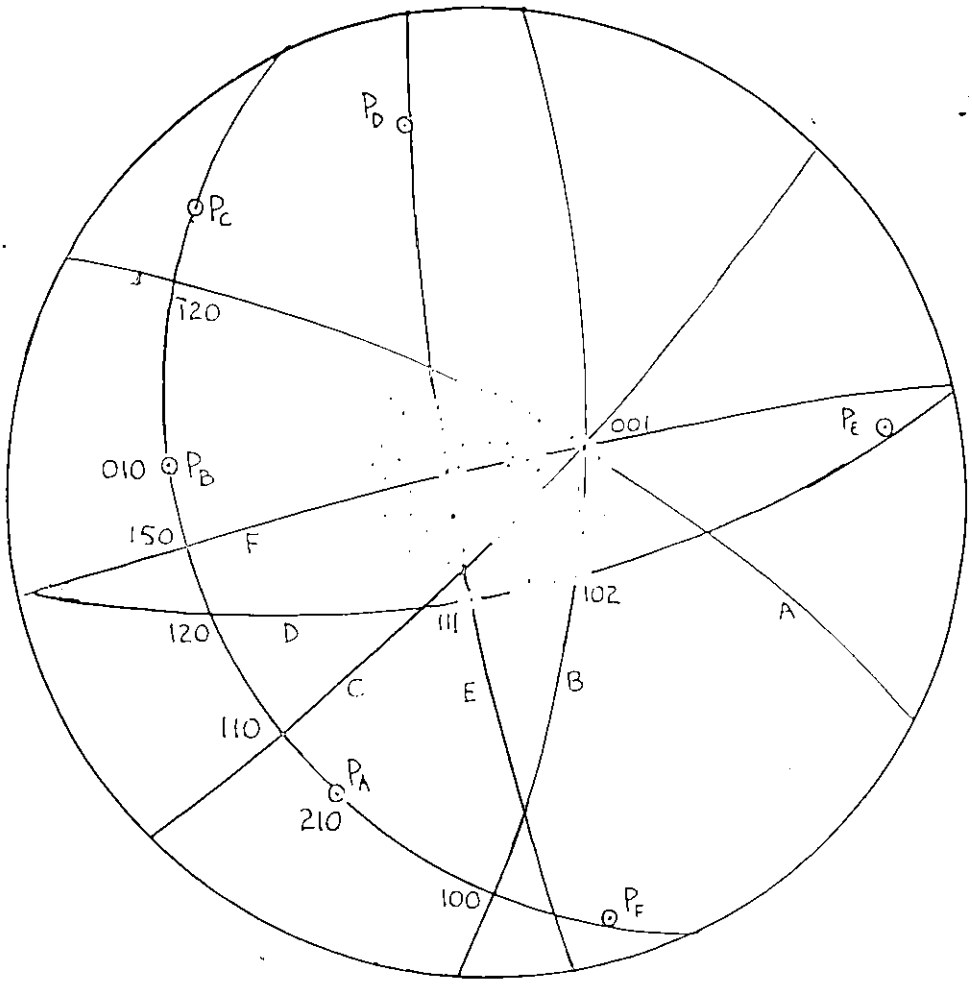

Figure 2.9 Stereographic projection of the single crystal photograph of Figure 2.8.

was a complete single crystal. This result suggests that another possibility would be to attempt growth at a slower rate.

Single crystal growth was then attempted with $Cd_xHg_yMn_zTe$ ($x + y + z = 1$). The first such sample, BR-9, broke almost like glass when attempts were made to cleave it. However, it too had a distinct orientation when examined using a Laue back-reflection X-ray picture.

A summary of the results of the growth of single crystals is given in table 2.1.

The second sample of CdHgMnTe exploded while annealing in the lower part of the furnace, necessitating the replacement of a number of furnace components. This unfortunate occurence was then used as an opportunity to relocate the furnace, add the extra heating coil (shown by arrow B in figure 2.3) and purchase three new high-precision temperature controllers. This process would stretch out to ten months due to difficulties with the controllers, so that no more single crystal growth was performed before the writing of this thesis.

2.5 Comparison of single crystals and polycrystalline samples

Four single-crystals grown by the Bridgman method, from samples BR-1, BR-2, BR-4 and BR-7, were compared with polycrystalline examples of the same nominal composition but grown by the melt and anneal method. Lattice parameters were measured by the Debye-Scherrer technique, while spin-glass transition temperatures were measured using the method described in section 3.3.2.

Table 2.1 SUMMARY OF CRYSTAL GROWTH BY THE BRIDGMAN METHOD

Sample ID	Nominal composition	Crystalline condition
BR-1	$Cd_{.225}Zn_{.075}Mn_{.7}Te$	Large grain* polycrystalline
BR-2	$Cd_{.7}Mn_{.3}Te$	Large grain polycrystalline
BR-3	$Cd_{.7}Mn_{.3}Te$	Large grain polycrystalline
BR-4	$Cd_{.6}Mn_{.4}Te$	Large grain polycrystalline
BR-5	$Cd_{.6}Mn_{.4}Te$	Large grain polycrystalline
BR-6 (new furnace)	$Cd_{.45}Zn_{.15}Mn_{.4}Te$	Large grain polycrystalline
BR-7	$Cd_{.3}Zn_{.3}Mn_{.4}Te$	Single crystal**
BR-8	$Cd_{.375}Zn_{.125}Mn_{.5}Te$	Single crystal
BR-9	$Cd_{.07}Hg_{.9}Mn_{.03}Te$	Large grain polycrystalline

* Grain size larger than the X-ray beam diameter of about 1 mm.

** Ingot size as drawn in figure 2.5.

The results for the single crystals were compared with values supplied by T. Donofrio (83B1, 85D1) for the polycrystalline samples, and are shown in Table 2.2.

As can be seen from the table, the characteristics of each single crystal sample are very close to those of its polycrystalline counterpart. For identical compositions, the characteristics should not differ. Thus the small differences may be attributed to slight differences in composition. For single crystals, these composition changes depend on the liquidus-solidus separation. For polycrystals, composition changes may be due to a deviation from uniformity over the entire ingot. The measurements which disagree the most are those of spin glass transition temperature for $Cd_{.7}Mn_{.3}Te$. But the deviation is accounted for if, for example, the manganese concentration is .33 in the single crystal, as opposed to the nominal concentration of .30.

The results thus indicate that the liquidus and solidus are very close in the CdZnMnTe system, as the grown crystal and the starting alloy have very close to the same composition.

2.6 Conclusions and recommendations

The following conclusions can be drawn from the work described in this section.

Single crystals of $Cd_xZn_yMn_zTe$ alloys ($x + y + z = 1$) can be grown by the Bridgman technique, when followed by a short annealing period.

Lattice parameter and spin glass-transition temperature characteristics of CdZnMnTe alloys are almost independent of whether they are single crystal or polycrystalline. This indicates that the star-

Table 2.2 Properties of single crystal and polycrystalline $Cd_xZn_yMn_zTe$

Composition	Lattice parameter (nm) ±0.005		Spin glass transition temperature (K)	
	Single crystal	Poly-crystalline	Single crystal	Poly-crystalline
$Cd_{.225}Zn_{.075}Mn_{.7}Te$	.6341	.6349	40±2	39±1
$Cd_{.7}Mn_{.3}Te$	.6431	.6438	9±0.5	7.1±0.5
$Cd_{.6}Mn_{.4}Te$	.6422	.6422	13±1	12±0.5
$Cd_{.3}Zn_{.3}Mn_{.4}Te$	.6360	.6306	13.7±0.5	13.2±0.5

ting alloy and grown crystal have close to the same composition. This result in turn means that there is only a small difference in temperature between the liquidus and solidus surfaces of the pseudo-ternary phase diagram. This result gives an important contribution to the knowledge of the form of the phase diagram for CdZnMnTe.

Single crystals, or at worst large-grain polycrystalline samples of $Cd_xHg_yMn_zTe$ ($x + y + z = 1$) can also be grown by the Bridgman method. However, prolonged high temperatures may cause these alloys to weaken their quartz containers and explode.

It is recommended that single crystal growth be continued, especially for research into the electrical properties of CdZnMnTe, and for electrical and optical work with CdHgMnTe. A method must be found to avoid explosion of the latter alloys, however.

THE EXCHANGE INTERACTION IN $Cd_xHg_yMn_zTe$ ($x + y + z = 1$)

3.1 Introduction

As stated in the introduction to this thesis, there are many different magnetic and magnetic field dependent effects observed in semimagnetic semiconductors. Any explanation of these effects must inevitably depend on a satisfactory description of the actual interaction which is taking place between the magnetic ions of the SMSC: the exchange interaction.

The exchange interaction can take place in many ways, depending on the conditions. Direct exchange, which depends on the overlap of the wave functions of the magnetic ions, is one form of the interaction. However, in semiconductor alloys, such as CdMnTe, the spacing of the magnetic cations is too large to allow for significant overlap. Thus direct exchange can be ruled out.

This leaves indirect exchange as the means by which magnetic ions interact in SMSC's (and in metallic alloys with low magnetic concentrations). Indirect exchange can occur through different mechanisms.

One such mechanism is the polarization of the electron gas, called the RKKY interaction. This requires a very high carrier concentration, and thus is not significant in materials other than metals and degenerate semiconductors (79B1).

The mechanism which has been deemed responsible for magnetic exchange in wide band gap SMSC's involves virtual transitions between the valence band and internal manganese energy levels (85L1). This

is commonly called superexchange. A more thorough description is given in section 3.2.1.

For SMSC's with smaller energy gaps, virtual transitions from the valence band to conduction band provide another medium for exchange to take place. This is called the Bloembergen-Rowland interaction and is the main subject of investigation in this thesis.

In both of the above cases for SMSC's, the resultant exchange interaction is antiferromagnetic (80L1).

At low temperatures, SMSC's display spin glass behavior, while paramagnetic behaviour is displayed at higher temperatures.

A spin glass is a "freezing" of spins into random orientations. This is accompanied by a cusp in the magnetic susceptibility measurements made as a function of temperature. However, no corresponding anomaly is observed in the specific heat (82G1).

In SMSC's, the random orientation of the spin glass is believed to be due to a lattice-induced "frustration" of the antiferromagnetic interaction (84B1). This frustration would result from the competing influences of two neighboring spins of opposite direction. This situation is depicted in figure 3.1. This contrasts with metallic spin glasses, where the oscillation with distance of the sign of the RKKY exchange interaction causes competition between antiferromagnetic and ferromagnetic interactions.

In addition to the random spin glass phase, an ordered antiferromagnetic phase has also been observed in SMSC's, but only with certainty in CdMnTe. Neutron diffraction studies showed that this alloy exhibited type III antiferromagnetic ordering for manganese concentration $z > 0.6$ (81G1). Short range ordering was also observed in

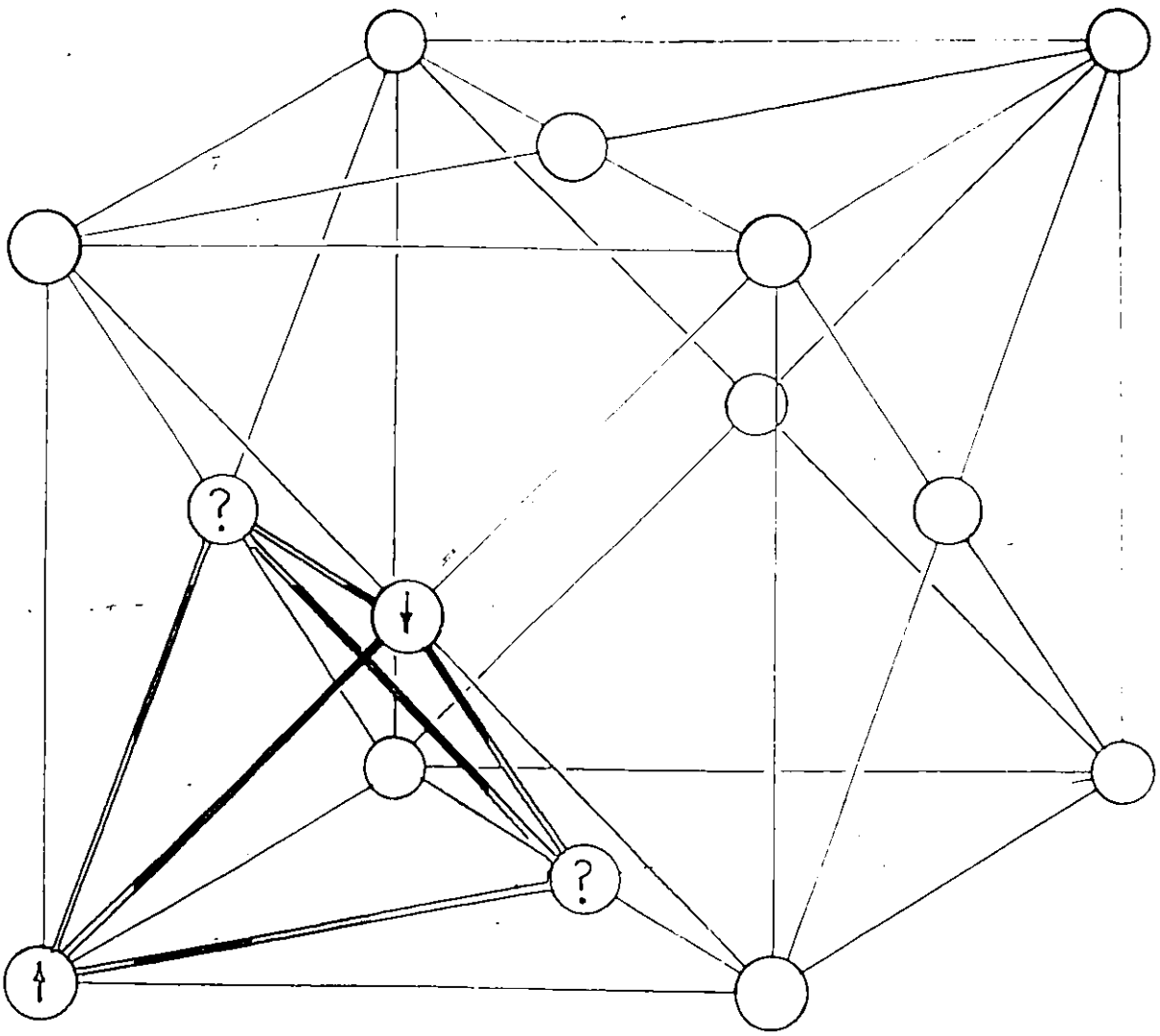

Figure 3.1 Depiction of the frustration of the antiferromagnetic interaction due to competition between equally spaced magnetic cations in the zinc blende structure.

ZnMnTe for z = 0.594 and 0.676 (82H1). Magnetic studies have indicated an antiferromagnetic phase for z > 0.6 in the pseudo-ternary alloy CdZnMnTe (85D1). The above alloys are the only SMSC's known to exist in a single crystallographic phase for concentrations of manganese high enough to result in antiferromagnetic ordering.

3.2 Theory

The temperature at which a SMSC becomes a spin glass is called the spin glass transition temperature, Tg. This transition from a paramagnetic to spin glass phase occurs when the thermal energy, kT, becomes less than the exchange energy (81E1, 84B1). The exchange energy between two magnetic ions separated by a distance r is (86W1).

$$E_{ex} = -S(S + 1)\ J(r) \qquad (3\text{-}1)$$

where J(r) is the exchange parameter

and S is the spin of each ion (=5/2 for manganese)

The transition is accompanied by a cusp in the susceptibility versus temperature curve. Hence Tg (and thus also the exchange energy) can be determined experimentally by measuring magnetic susceptibility as a function of temperature.

3.2.1 Wide Gap SMSC's

In a wide gap semiconductor such as CdMnTe, the exchange energy has been attributed to indirect exchange via the manganese $3d^6$ level, called superexchange (85L1). Specifically, a virtual transition occurs from the full valence band to the de-localized manganese $3d^5$

level. This results in a hole in the valence band and a manganese $3d^6$ electron. Because the valence band, which has p character, now has a net magnetic moment due to the hole, it can interact magnetically with another neighboring manganese atom.

The form of this interaction has been derived theoretically by Geertsma et al. (77G1). Their result for the exchange parameter J(r) is:

$$J_G(r) = \frac{I_o}{r^2} \exp(-\alpha r) \qquad (3\text{-}2)$$

$$\text{with } \alpha = 2(2m^*\epsilon/\hbar^2)^{\frac{1}{2}}$$

where: m^* is the valence band effective mass

ϵ is the difference in energy between the valence band and the Mn $3d^6$ level.

I_o is a constant

and r is the distance between the magnetic ions.

The constants I_o and α in equation 3-2 have been determined experimentally (86W1). This was done by using a mean value for the manganese-manganese distance r, as suggested by Escorne et al. (81E1). The value used was $r_m = dz^{-1/3}$ where d is the nearest neighbor cation distance and z the manganese concentration. The value of d was given by the lattice parameter a as $d = a/\sqrt{2}$ for zinc blende and $d = a$ for wurtzite. Equating the thermal energy kTg with the exchange energy of 3-1 gives:

$$kT_g = -S(S+1)\frac{I_o}{r^2}\exp(-\alpha r_m) \qquad (3\text{-}3)$$

$$\text{or} \quad \log(r_m^2 T_g) = \log\frac{-S(S+1)I_o}{k} - \alpha r_m \qquad (3\text{-}4)$$

It was found that plotting $\log(r_m^2 T)$ versus r_m resulted in straight lines whose slope, $-\alpha$, and intercept, $\log(-S(S+1)I_o/k)$, were independent of the actual alloy but dependent upon the crystal structure. For the zinc blende alloys CdZnMnTe and CdMnTeSe the values obtained were:

$$\frac{-S(S+1)I_o}{k} = (2.03 \pm 0.5) \times 10^2 \text{ K}\cdot\text{nm}^2$$

and $\alpha = 6.1 \pm 0.4 \text{ nm}^{-1}$

Different values were obtained for alloys with the hexagonal wurtzite structure.

Using these constants and equation 3-3 it should be possible to predict spin glass transition temperatures for any wide band gap SMSC, given the structure, lattice parameter and manganese concentration. A plot of transition temperature versus manganese concentration using equation 3-3 and the above constants is given in figure 3.2 for a hypothetical wide-band gap SMSC with zinc blende structure. This will prove useful in the analysis of narrow gap SMSC's, when it is necessary to determine the change in the exchange energy due solely to the smaller energy gap. The narrow gap exchange energy will be taken as the difference between the measured energy and the amount predicted through equation 3.3 as resulting from the normal wide gap interaction.

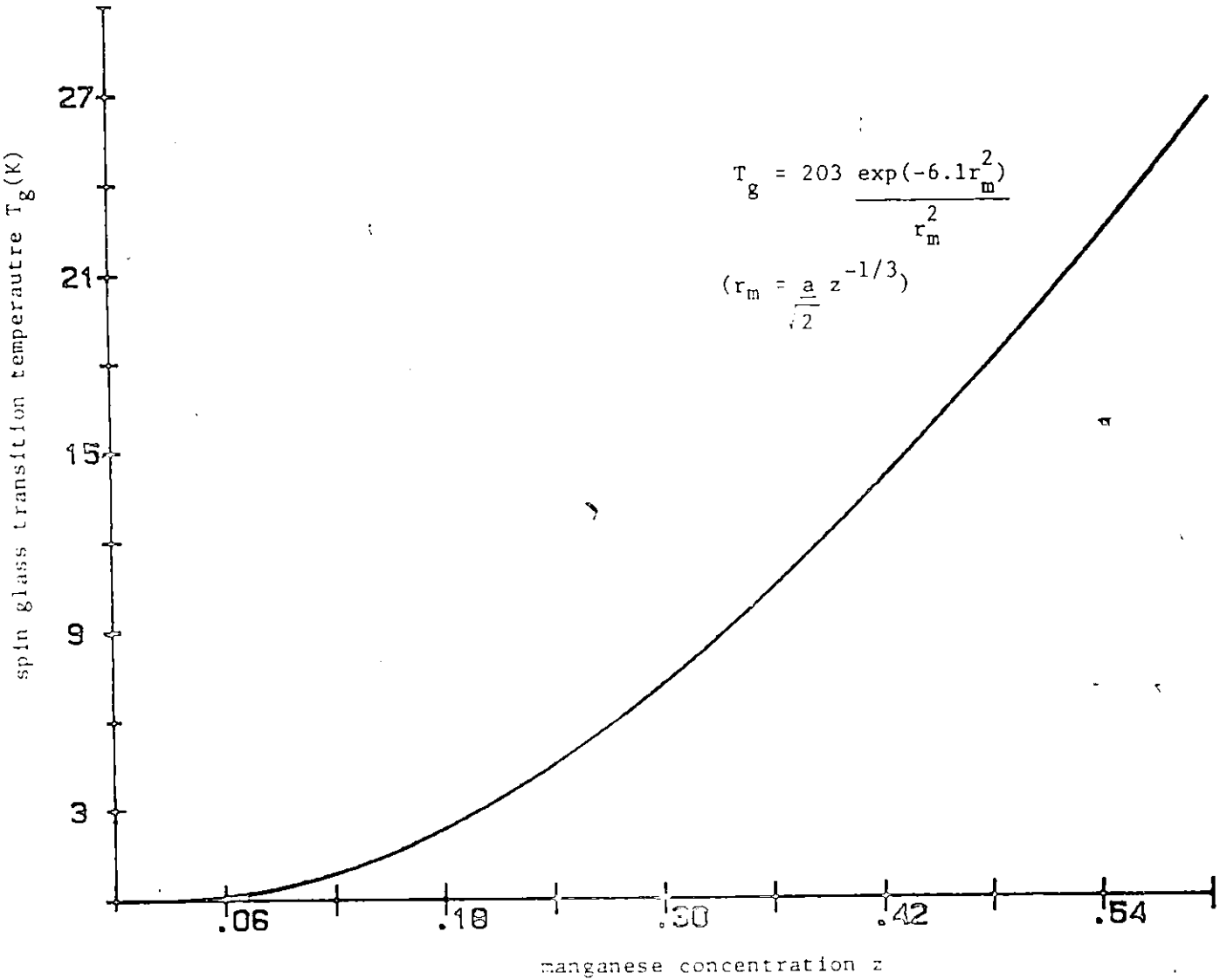

Figure 3.2 Example of spin glass transition temperature versus manganese concentration using equation 3-3 and the fitted parameters given on page 32 with the lattice parameter arbitrarily set to a = 0.6400.

3.2.2 Narrow gap SMSC's

When the energy gap, Eg, between the valence and conduction bands becomes small, virtual transitions across the gap result in another form of the exchange interaction. This is called the Bloembergen-Rowland interaction, after the authors who first derived a description of it in 1955 (55Bl). Their result for the exchange parameter J(r) is:

$$J_{B1}(r) = \frac{C}{r^3} \exp[-(\alpha_1)r] \qquad (3\text{-}5.a)$$

$$\text{with } \alpha_1 = (2m_c Eg/\hbar^2)^{\frac{1}{2}}$$

where C = constant

m_c = conduction band effective mass

E_g = energy gap.

However, m_c depends on the energy gap. For low E_g using the Kane model (72Bl), we get $m_c = LE_g$, where L is a constant.

Thus $\alpha_1 = (2L/\hbar^2)^{\frac{1}{2}} Eg$ (3-5.b)

More recently (1980), Abrikosov (80Al) has given a new derivation, along with comments on the methods of Bloembergen and Rowland. His result for the exchange parameter is:

$$J_{B2}(r) = \frac{C_1}{r^{5/2}} (\alpha_2 m^*)^{3/2} [2(m_e + m_h)]^{-1/2} \exp(-\alpha_2 r) \qquad (3\text{-}6)$$

$$\text{with} \quad \alpha_2 = (2(m_e + m_h)E_g/\hbar^2)^{1/2}$$

where C_1 = constant

m_e, m_h = electron and hole effective masses

$m^* = (m_e^{-1} + m_h^{-1})^{-1}$

E_g = energy gap

Again, since E_g is small, $m^* \simeq m_c$ so that

$$m^* \propto E_g$$

Thus,

$$J_{B2}(r) = C_2 E_g^{9/4} r^{-5/2} \exp(-\alpha_2 r) \qquad (3\text{-}7)$$

where C_2 = constant

Abrikosov's derivation was made for small concentrations of the magnetic component. No theoretical work on the whole range of magnetic concentration could be found.

The next step to take is to find out how to determine the contribution of the Bloembergen-Rowland interaction to the overall exchange energy.

If one assumes that the two interactions are independent (85L1), then the total exchange energy is simply a sum of the wide band gap exchange energy given in equation 3-3 and the narrow gap exchange energy. Thus the total exchange parameter $J_T(r)$ will be given by

$$J_T(r) = J_G(r) + J_B(r) \qquad (3\text{-}8)$$

Equating the thermal energy at the transition temperature to the exchange energy, as in equation 3-3, gives:

$$kT_g = -S(S + 1)J_T(r)$$

One can write:

$$T_g = -\frac{AJ_G(r)}{k} - \frac{AJ_B(r)}{k} \qquad (3\text{-}9)$$

where $A = S(S + 1)$

or:

$$T_d = -\frac{AJ_B(r)}{k} \qquad (3\text{-}10)$$

with $T_d = T_g - T_{gG}$ being the difference between the

spin glass transition temperature of the narrow gap SMSC, and T_{gG}, the transition temperature that would occur if only the wide gap interaction of equations 3-2 and 3-3 was important.

3.3 Experiment

As shown in figure 1.1 on page 4, the energy gap of the CdHgMnTe alloy system goes to zero near the HgTe corner of the ternary diagram. This characteristic makes this alloy system suitable for studying the exchange interaction in SMSC's with a low band gap. Another factor in favour of this alloy system is the wide range over which a single phase should exist, as the three pseudo-binary alloys which make up this system all have large ranges of solid solution. These are: $Cd_{1-z}Mn_zTe$, which is zinc blende up to z = 0.74 (81T1); $Cd_{1-x}Hg_xTe$, which is single phase for the entire range of x (60W1); and $Hg_{1-z}Mn_zTe$ which definitely exists in the zinc blende phase up to z = 0.35, and possibly up to about z = 0.75 (63D1).

Another student in the semiconductor laboratory at the University of Ottawa, Sudershan Manhas, is currently working on the phase diagram, crystallography, magnetic and ESR properties of the entire CdHgMnTe system. However, his work had not been completed at the time of writing this thesis.

Since this study is concerned with the effect of a low energy gap, only samples near the mercury telluride corner were prepared. For comparison purposes, two wide gap samples, provided by Mr. Manhas were also studied. Mr. T. Donofrio, also of the semiconductor laboratory, provided data for two points on the CdMnTe edge of the alloy system.

3.3.1 Sample Preparation

The melt and anneal method was used to prepare all of the alloys for this investigation. Constituents were weighed out to make 1.5 g. samples to a precision of better from five parts per thousand. In all, fifty-one samples were made. The constituents were weighed in elemental form, except for mercury. Mercury was first reacted separately with tellurium, at a relatively low temperature of 500°C, to form mercury telluride. This was done to aid in the weighing, and to minimize the vapour pressure due to free mercury at higher temperatures.

The components were then sealed with an oxy-acetylene torch into quartz tubes which had been evacuated to less than 0.1 pascal. The lower part of the inside of each of the quartz tubes was first coated with carbon by cracking acetone over a Bunsen burner. This was done to prevent the manganese from reacting with the quartz during the melting operation.

The sealed tubes were then heated to 1100°C over a one hour period, and kept at that temperature for about 15 minutes. After cooling overnight, the tubes were then placed for one month in annealing furnaces set at 550°C. The annealing furnaces were allowed to cool overnight before the tubes were removed.

The quartz tubes were broken open, and the contents were carefully inspected. In almost all of the cases, a small amount of free mercury was observed. It was assumed that the mercury had evolved from the top portion of the ingot. For this reason, only the bottom third of the ingots were used for analysis. Also, many samples were

rejected because of their appearance: they were too porous, or they had separated into two dissimilar pieces, etc.

Debye-Scherrer powder X-ray photographs were then taken of each sample, and the lattice parameters were measured. In all cases, the X-ray pictures identified the structure of the samples to be zinc blende type. In a few cases, the existence of a second phase was revealed by the presence of a diffraction pattern in addition to that of the zinc blende structure. This pattern was always very faint, indicating that the second phase existed at most in quantities around 5%.

3.3.2 Measurement of the spin glass transition temperature, T_g

The temperature at which a sample undergoes transition between the paramagnetic phase and a spin glass phase can be determined by measuring the d.c. magnetic susceptibility as a function of temperature. At the transition temperature, T_g, a cusp is evident in the otherwise smoothly varying curve. This discontinuity in the slope is attributed to the "freezing" of the spin orientations, similar to the Néel temperature in the case of an antiferromagnetic substance. In the spin glass case, however, the spins freeze into a disordered state.

The actual measurement of susceptibility was performed using the equipment of Dr. G. Lamarche of the University of Ottawa. A schematic diagram is given in figure 3.3. It consists of a variable-temperature cryostat into which a moveable sample holder is inserted. Surrounding this is a cryostat kept at liquid helium temperature.

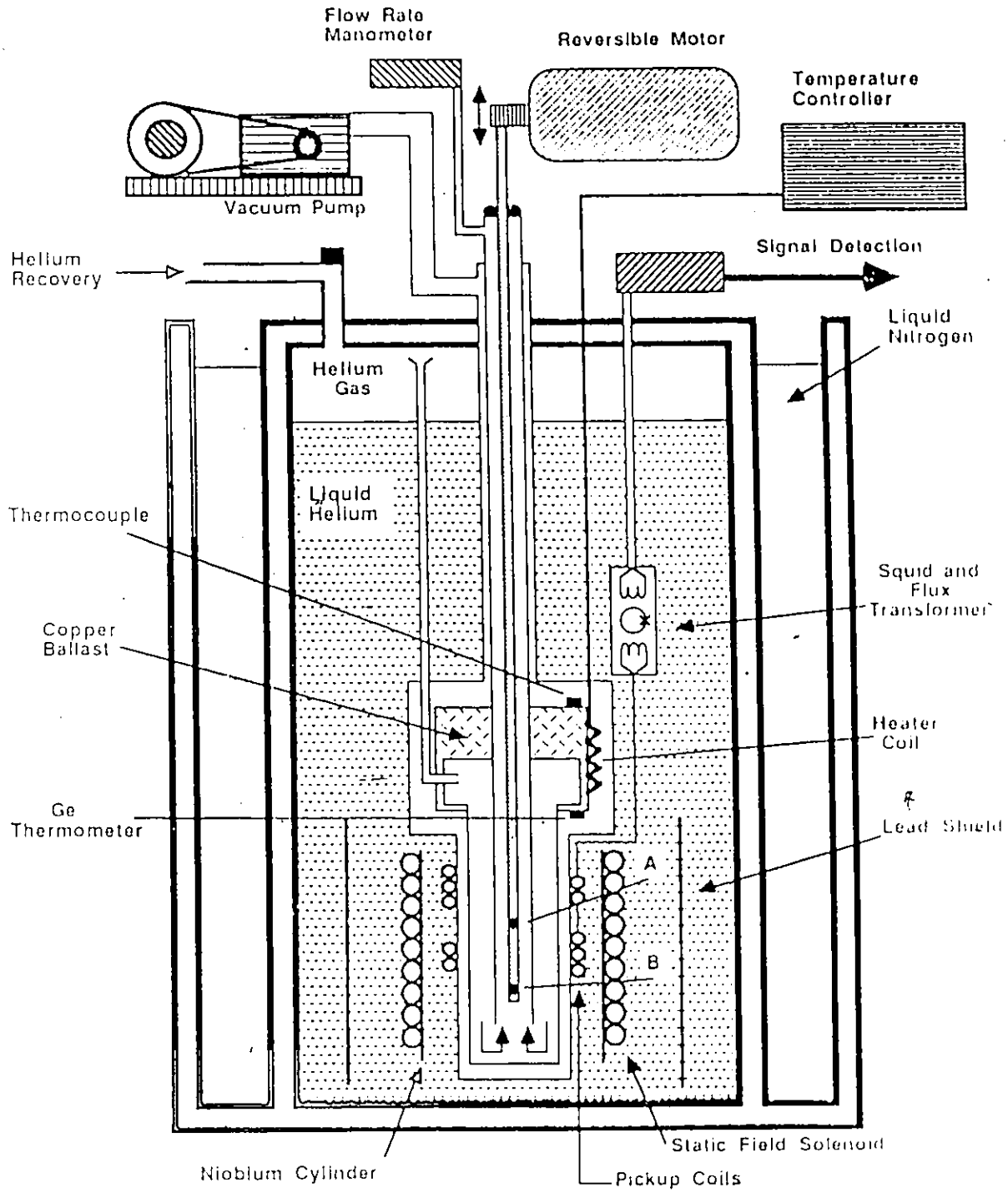

Figure 3.3 Schematic diagram of the equipment used to measure d.c. magnetic susceptibility. Samples go in positions A and B. Diagram courtesy of T. Donofrio.

This outer cryostat contains a superconducting niobium cylinder to trap magnetic fields of known strength, and two superconducting coils wound in opposite directions. These coils are connected to a SQUID (superconducting quantum interference device).

The sample holder is lowered at a slow speed through the two coils. This results in a current change in the coil to counteract the flux change arising from the magnetisation of the sample. This current is amplified through the SQUID, and the output voltage fed into a computer. The computer averages the values for an upward and then downward pass of the sample holder, converts the voltage into units of susceptibility and stores the results along with the temperature reading. The susceptibility is then plotted as a function of temperature. A typical result is shown in Figure 3.4.

It should be noted that the values of susceptibility below T_g are dependent on whether the sample was cooled in or out of the magnetic field. Samples cooled in the field have a higher susceptibility below T_g, while above T_g they act the same as samples cooled in zero field. Normally, it is more difficult to determine the position of the cusp in the susceptibility-temperature curve for a field-cooled sample. For this reason, zero-field-cooled measurements are usually made first. If the cusp has been blurred out, perhaps by a slight inhomogeneity in the sample, then field-cooled measurements are made, and T_g is taken to be the temperature at which the curves intersect.

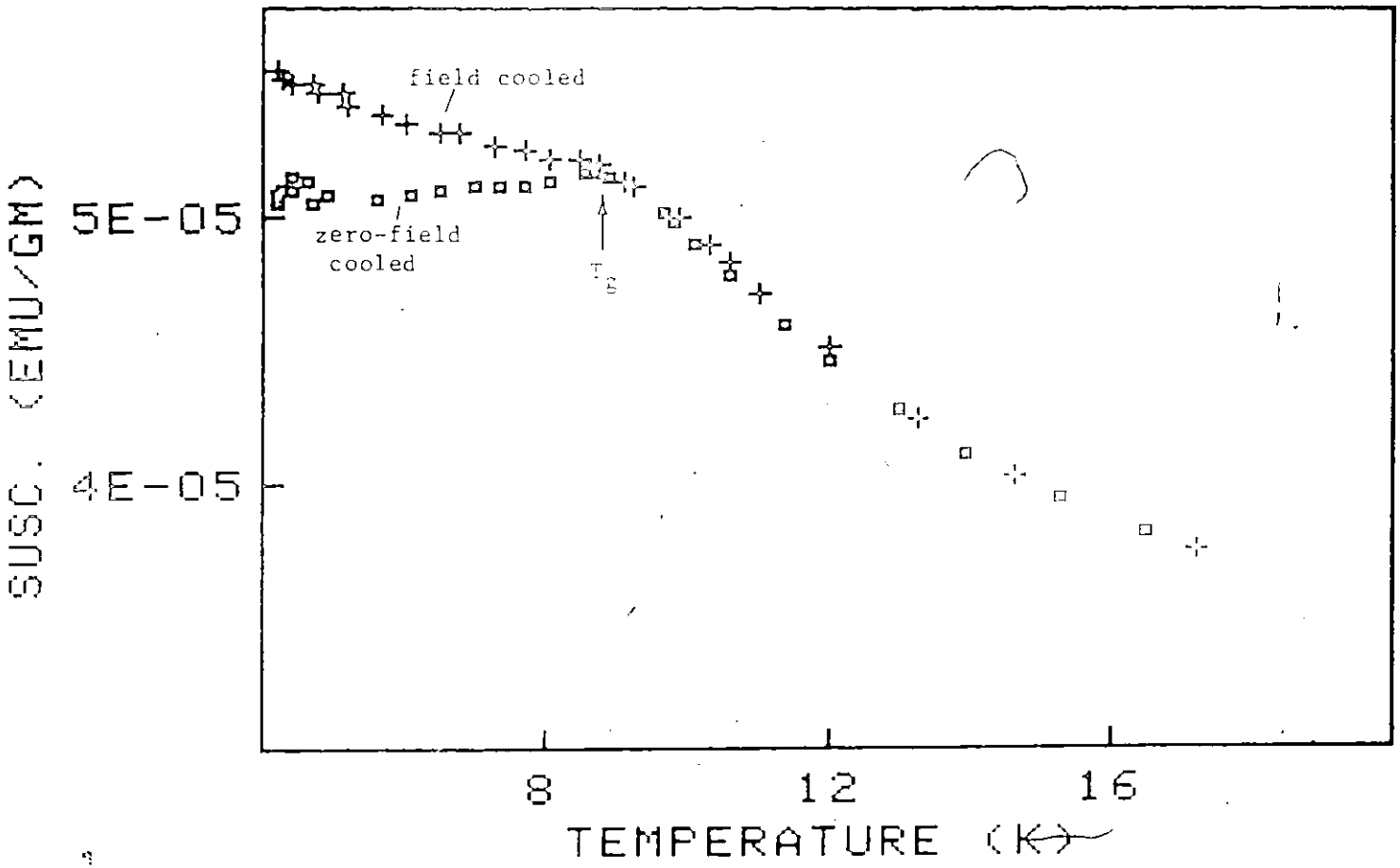

Figure 3.4 A typical graph of magnetic susceptibility versus temperature for a semimagnetic semiconductor. This graph is of data for sample S2 and shows both zero-field cooled and field cooled results, as plotted by the computer interfaced with the measurement apparatus.

3.3.3 Measurement of the energy band gap, E_g, by optical absorption

In order to measure the energy band gap of the various samples, the procedure described by Goodchild et al. (82G2) was followed. This method uses the relationship between the absorption coefficient and the photon energy $h\nu$ at the absorption edge:

$$\alpha h\nu = A(h\nu - E_g)^n \qquad (3\text{-}11)$$

where A = constant

n = ½ for a direct allowed transition

2 for an indirect allowed transition

3/2 for a direct forbidden transition

and 3 for an indirect forbidden transition

A thin slice of each sample was cut using a wire saw, and then was ground down to between 150 and 350 μm using alumina and silica powders. The thinned piece was then mounted covering a hole in an aluminum plate. The edges and any visible holes in the sample were blocked with silver print.

The absorption coefficient was determined by measuring both the incident and transmitted light intensity, I_o and I_T, as a function of wavelength.

For wavelengths up to 3 μm, a 30 W tungsten ribbon lamp was used as the light source. For lower energy gap samples, the light source used was a 40 W tungsten filament lamp with a quartz bulb. This allowed measurements out to about 4.2 μm.

The monochromator used was a Spex 1702, with Bausch and Lomb gratings blazed at 1.6 μm and 4 μm, depending on the desired wavelength range. The light was filtered at the output slit of the monochromator to remove the higher orders of the short wavelengths present. Colour or dielectric filters of the appropriate cutoff wavelengths were used.

Light from the monochromator was then focused on the sample, and the transmitted light detected with a Dumont 6911 photomultiplier, a biased PbS cell, or a Laser Precision kT-2220 pyroelectric detector. To obtain the incident intensity, the light was simply allowed to fall on the hole in the aluminium plate, with no sample in place, so that the same area as the sample was illuminated.

The detector output was fed into a lock-in amplifier. A PAR 186A, 128A or 129 lock-in was used depending on availability. Preamplification of the signals from the PbS cell and the pyroelectric detector was obtained using either a PAR 113 roll-off amplifier or a PAR 189 selective amplifier.

The sample thickness, d, was measured with a micrometer, and a graph of $\frac{1}{d} \log (I_0/I_T)$ versus photon energy was made. A linear extrapolation of the background absorption was then subtracted and the difference was taken to be absorption due to interband transitions.

The maximum values of α measured were in the range 500 to 730 cm^{-1}, which indicate a direct allowed transition. Thus $n = \frac{1}{2}$ in equation 3-11, and graphs were made of $(\alpha h\nu)^2$ versus $h\nu$. The

straight line portion was extrapolated to give the $h\nu$ intercept. From equation 3-11, it can be seen that this intercept is the value of the energy gap.

An example of this procedure is given for sample M15 in figure 3.5.

3.4 Results and analysis

In order to clearly observe the behaviour of the low band-gap SMSC's, it was decided to concentrate on specific compositions of the alloy. What was needed was to vary the energy gap over a wide range, while holding constant as many parameters as possible.

These constraints led to the choice of the compositions containing constant manganese concentrations of 0.25 and 0.3, and to the HgMnTe edge of the pseudo-ternary alloy (i.e. no cadmium).

Some samples which duplicated other samples (made as backups) were also found to be unnecessary.

After the X-ray, magnetic and optical measurements had been made, graphs were plotted of the raw data points to determine their suitability for further analysis. The criterion for this suitability was that for alloys within a given phase field, the values should vary smoothly with composition. Any point which did not form part of a smoothly varying curve was rejected. The reason for the deviation was assumed to be a change in composition due to a large scale inhomogeneity in the sample or to the presence of a second phase in large quantities.

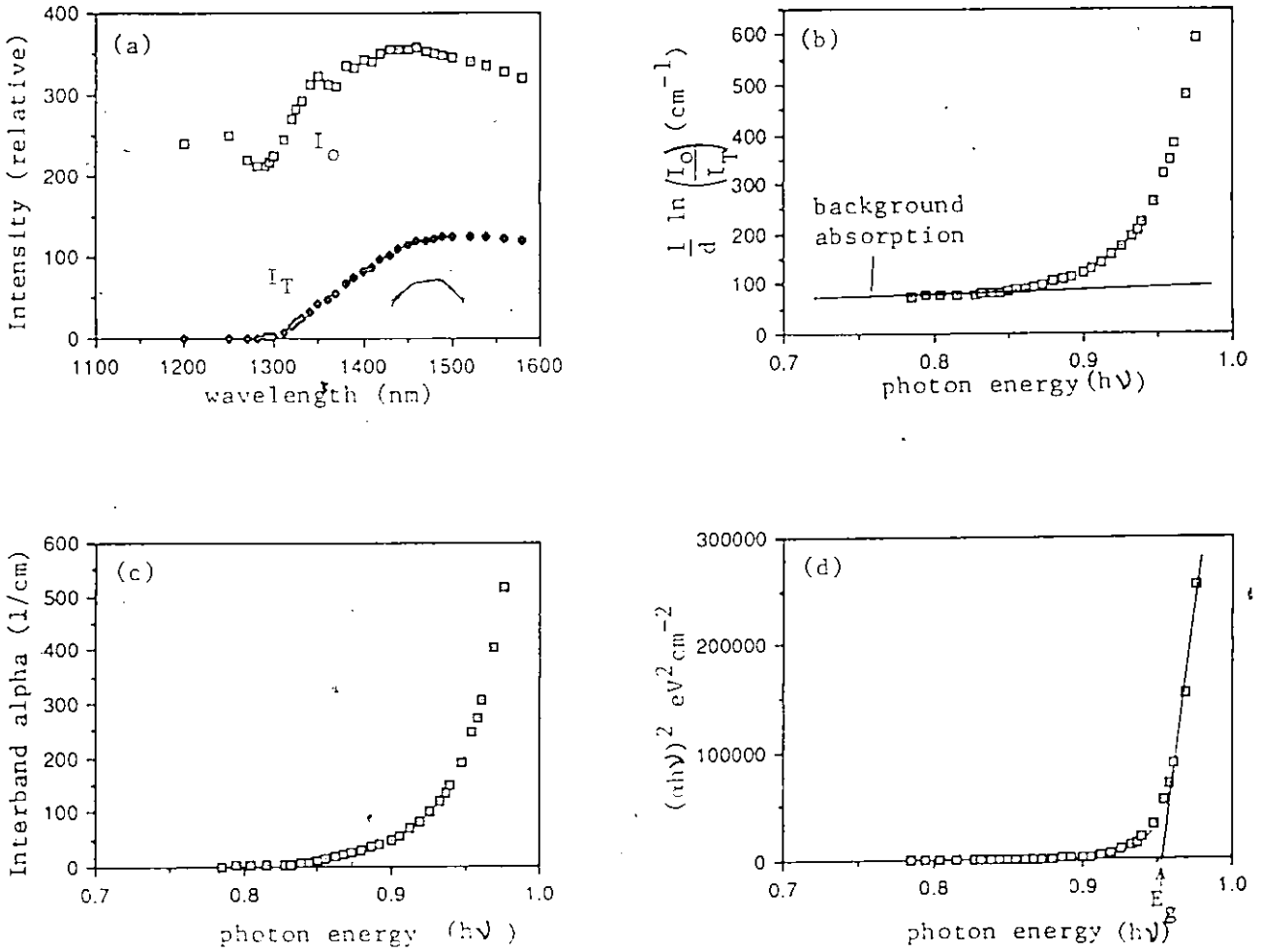

Figure 3.5 Diagrams showing the steps in determining the energy gap by optical absorption: a) Incident and transmitted intensities versus wavelength b) 1/d ln (I_o/I_T) versus photon energy, and extrapolated background absorption; c) interband absorption versus photon energy; and d) $(\alpha h\nu)^2$ versus photon energy and line extrapolated to the energy gap.

Graphs were plotted of the following quantities: Eg and Tg versus z for the mercury edge $Hg_{1-z}Mn_zTe$; and Eg and Tg versus the cadmium fraction of the non-magnetic cations, $\frac{x}{x+y}$ for constant manganese concentrations of z = 0.3 and z = 0.25. These graphs are shown in figures 3.6 to 3.8.

From the graphs, it can be seen that the results are fairly consistent. The bad samples are easily identified, and are not included in further analysis. The values of lattice parameter, energy gap and spin glass transition temperature of the remaining samples are given in Table 3.1.

An interesting result is shown by figures 3.7(b) and 3.8(b). Effectively, the only parameter being varied in these cases is the energy gap. Both the magnetic component (manganese) and the lattice parameter are constant. However, the spin glass transition temperatures decreases as mercury is replaced by cadmium and the energy gap is increased. This is a good indication of the significance of the Bloembergen-Rowland interaction in the total interaction energy.

Using equation 3-3, calculations were made of T_{gG} the spin glass transition temperatures corresponding to semiconductors of the same lattice parameters and manganese concentrations as those of the experimental samples, but with wide band gaps. The parameters used in this equation were obtained from alloys whose energy gaps were greater than 1.5 eV, meaning they had negligible contribution to their exchange energies from the Bloembergen-Rowland interaction.

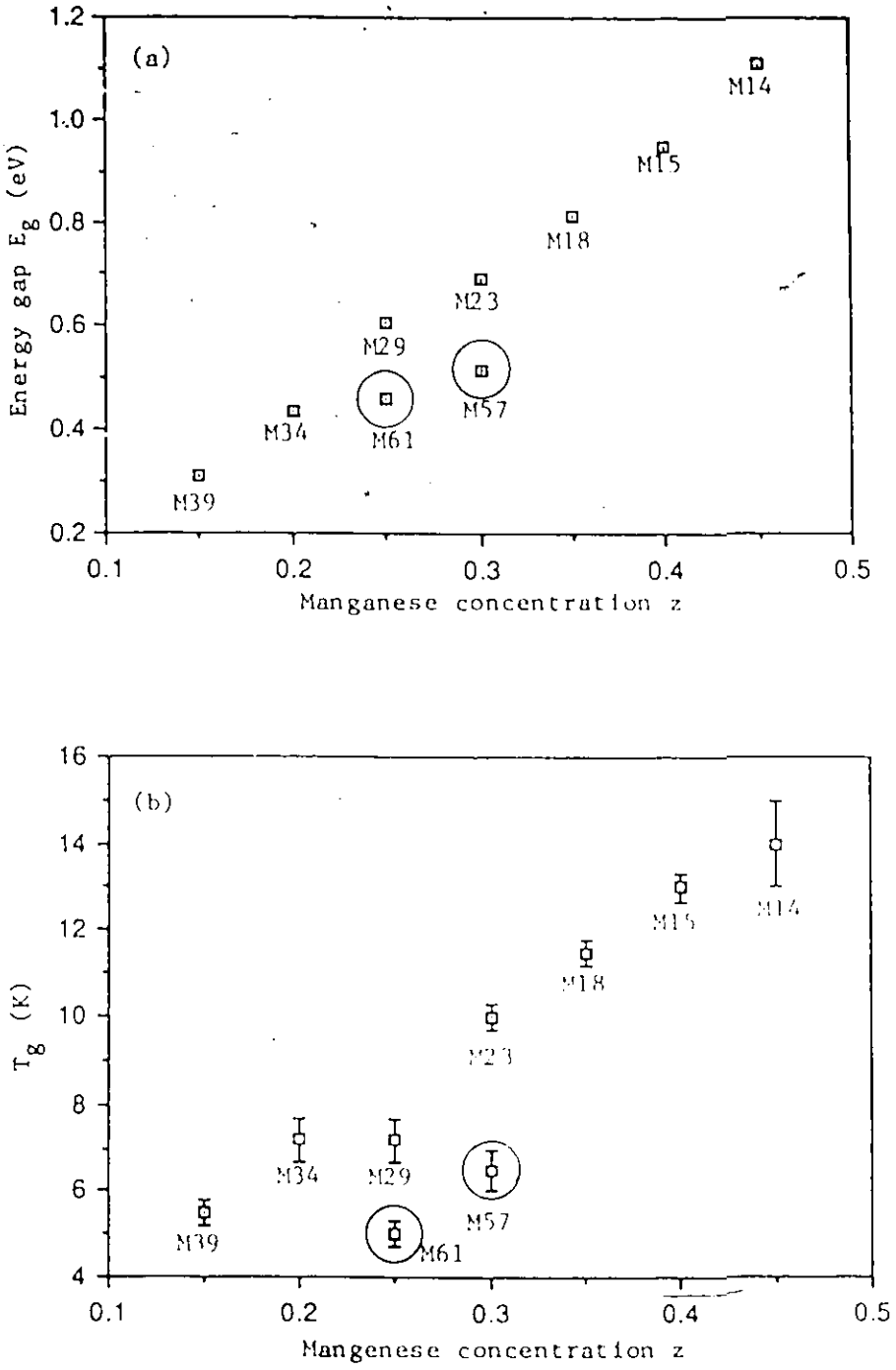

Figure 3.6 Graph of (a) energy gap E_g and (b) spin glass transition temperature T_g versus manganese concentration z for the $Hg_{1-z}Mn_zTe$ edge of the CdHgMnTe alloy system. Rejected points are circled.

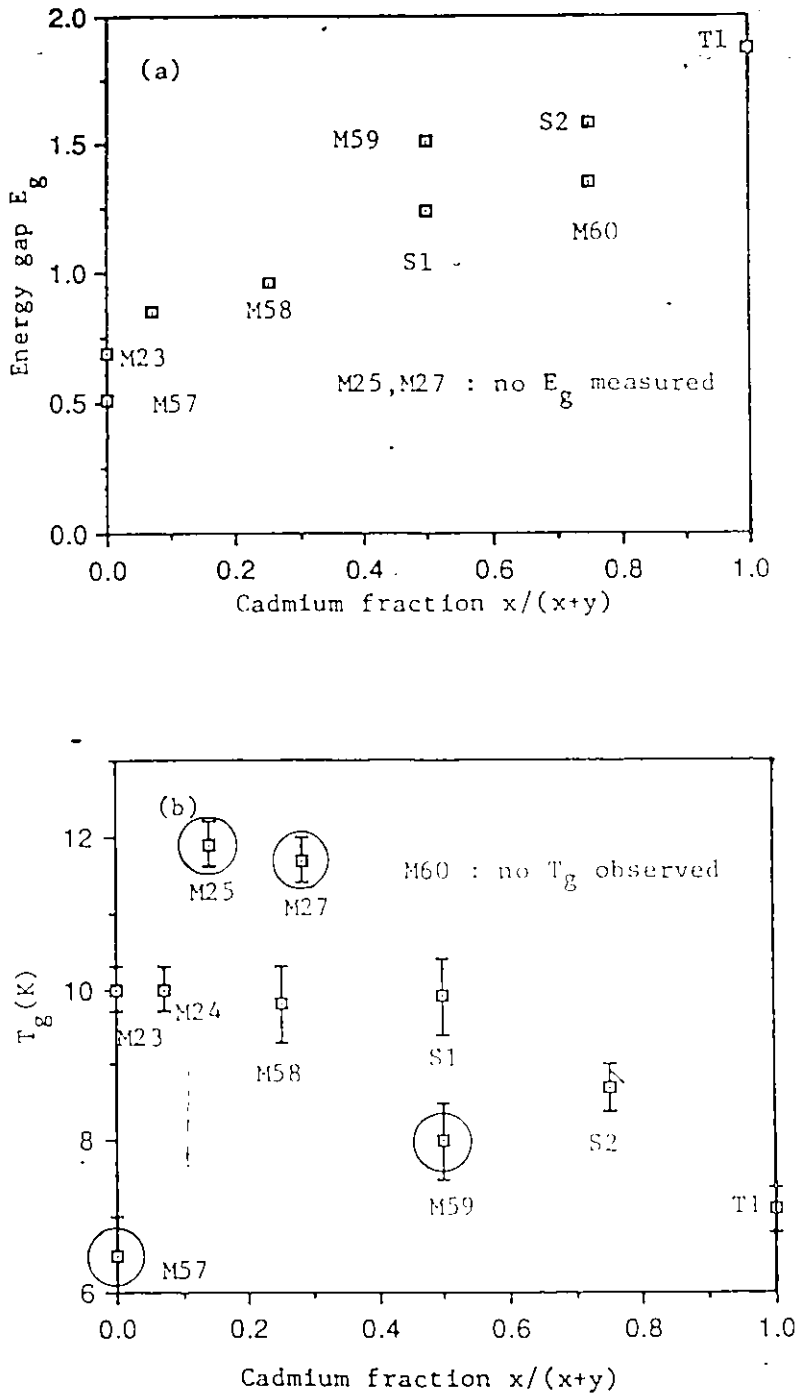

Figure 3.7 Graph of (a) energy gap E_g and (b) spin glass transition temperature T_g versus $\frac{x}{x+y}$, the cadmium fraction of the non-magnetic cations for the compositions $Cu_xHg_yMn_{.3}Te$ (x+y=0.7). Rejected points are circled.

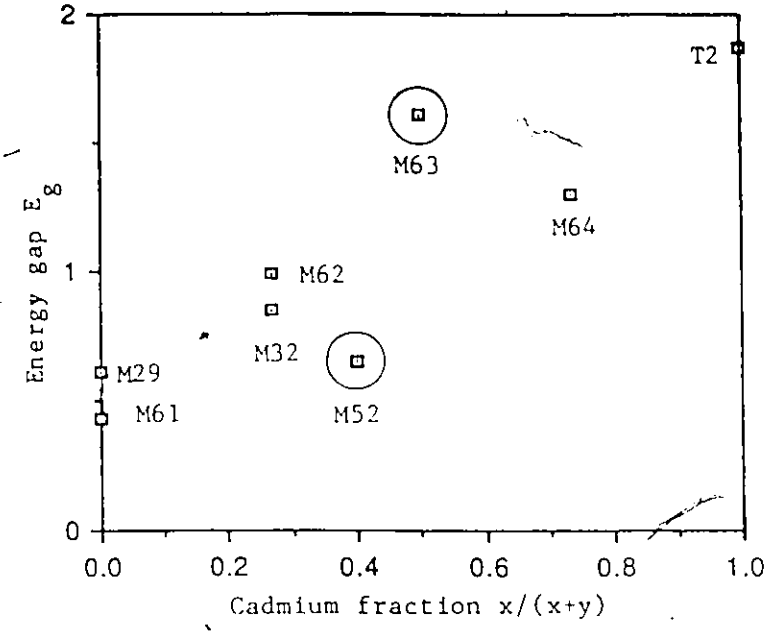

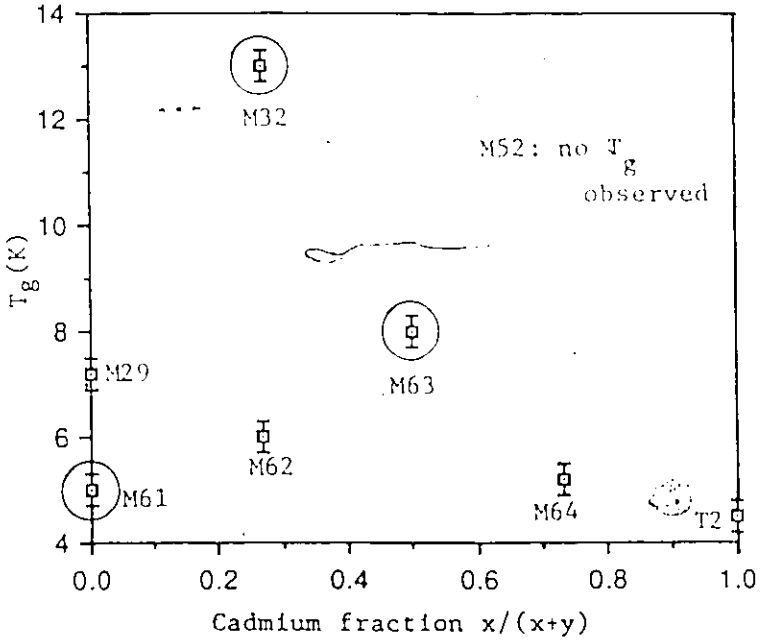

Figure 3.8 Graph of (a) energy gap E_g and (b) spin glass transition temperature T_g versus $\frac{x}{x+y}$, the cadmium fraction of the non-magnetic cations for the compositions $Cd_xMg_yMn_{.25}Te$ (x+y=0.75). Rejected points are circled.

Table 3.1 Lattice parameter, energy gap and spin glass transition temperature of samples used for the analysis of small-gap exchange interaction

Sample	Composition x - y - z	Lattice Parameter (nm) ±0.0005	Optical Energy Gap (ev) ±0.02	Spin glass Transition Temperature (K) ± 0.3
M14	0 - .55 - .45	.6427	1.11	15 ± 1
M15	0 - .60 - .40	.6413	0.95	13
M18	0 - .65 - .35	.6413	0.82	11.5
M23	0 - .70 - .30	.6418	0.69	10
M24	.05 - .65 - .30	.6422	0.85	10
M29	0 - .75 - .25	.6425	0.61	7.2
M34	0 - .80 - .20	.6433	0.43	7.2
M39	0 - .85 - .15	.6445	0.31	5.5 ± 0.5
M58	.175 - .525 - .30	.6418	0.96	9.8
M62	.20 - .55 - .25	.6421	0.99	6.0
M64	.55 - .20 - .25	.6451	1.30	5.2
S1	.35 - .35 - .30	.6428	1.24	9.9
S2	.525 - .175 - .30	.6431	1.58	8.7
T1	.70 - 0 - .30	.6438	1.93	7.1
T2*	.75 - 0 - .25	.6445	1.87	4.5

* Lattice parameter and energy gap interpolated, spin glass transition temperature extrapolated from data furnished by T. Donofrio.

These temperatures were then subtracted from the experimental values of T_g. The difference T_d was considered to be due solely to the Bloembergen-Rowland effect. This procedure is illustrated for the $Hg_{1-z}Mn_zTe$ samples in Figure 3.9.

These temperature differences were analysed according to the theoretical predictions of equation 3-7.

$$J_{B2}(r) = \frac{C_2}{r^{5/2}} E_g^{9/4} \exp(-\alpha_2 r)$$

$$\text{with } \alpha_2 = (2(m_e + m_h)E_g/\hbar^2)^{\frac{1}{2}}$$

The quantity $\log(r^{5/2} E_g^{-9/4} T_d)$ was plotted against $E_g^{\frac{1}{2}} r$. This graph is given in Figure 3.10. The slope of this line is $a = -12.2 \pm 4.5$ $eV^{-\frac{1}{2}}nm^{-1}$. This gives a value for the sum of the effective masses $m_e + m_h = 5.7 \pm 4.2$ m_o.

The expected value of $m_e + m_h$ is between $0.3m_o$ and 0.8 m_o using the data for HgTe and CdTe given by Long and Schmit (70L1 p. 197, 201) and Moss, Burrell and Ellis (73M1 p. 398, 399). Thus the value obtained using the formula of Abrikosov is about a factor of ten higher than predicted.

When instead the original Bloembergen-Rowland formula is used (equation 3-5) and a graph of $\log(r^3 T_d)$ versus $E_g \cdot r$ is plotted as shown in figure 3.11, the slope is found to be $a = -2.1 \pm 0.9$ $eV^{-1}nm^{-1}$. Using equation 3-5(b), this gives $L = 10 \pm 8 \times 10^{-13} s^2 m^{-2}$. Data given for CdHgTe (73M1 p. 397, 398) results in a value of $L = 6.7 \pm 0.3 \times 10^{-13} s^2 m^{-2}$. These results are thus in better agreement than those obtained using the theory of Abrikosov.

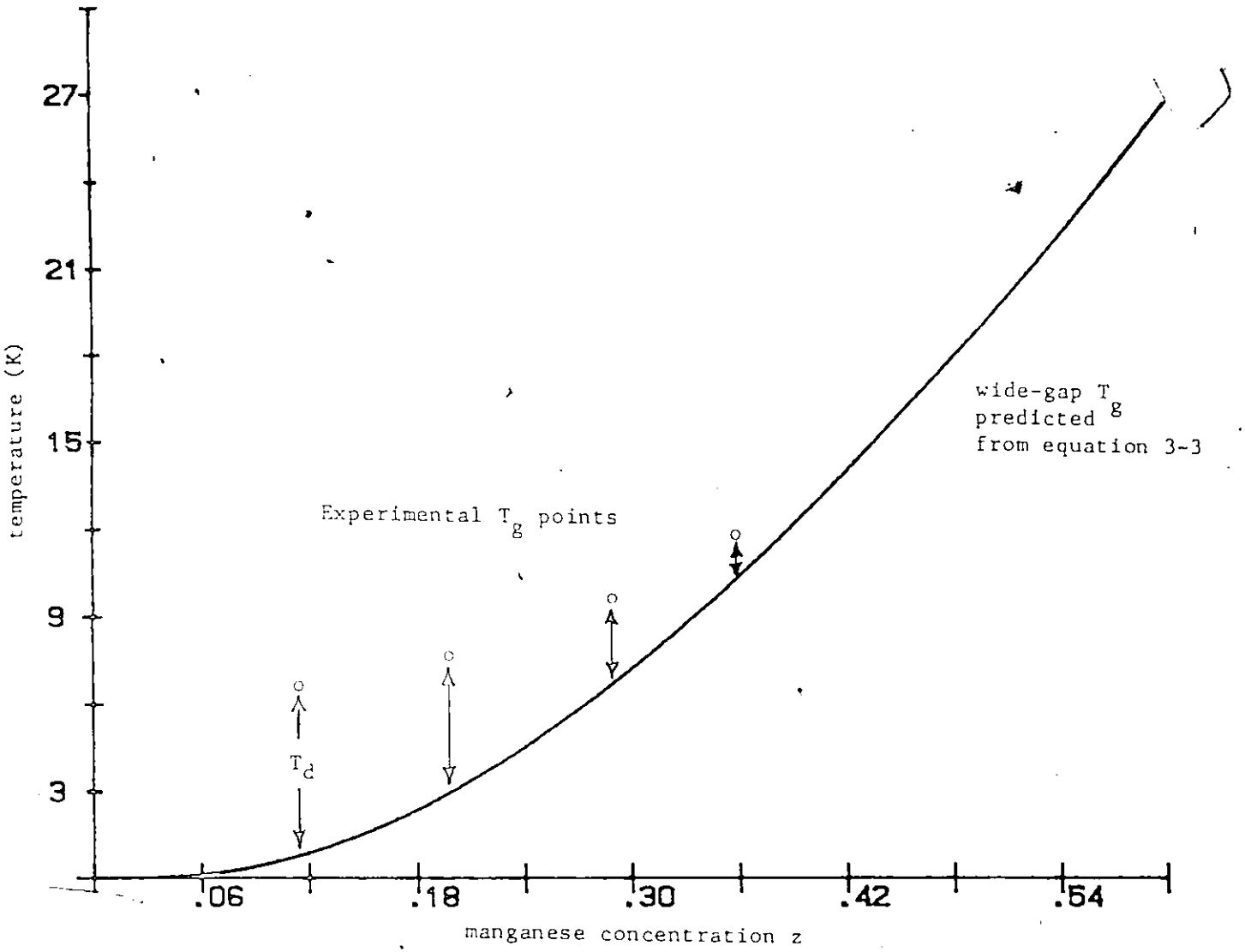

Figure 3.9 Diagram showing the procedure used to calculate the temperature difference T_d for hypothetical points.

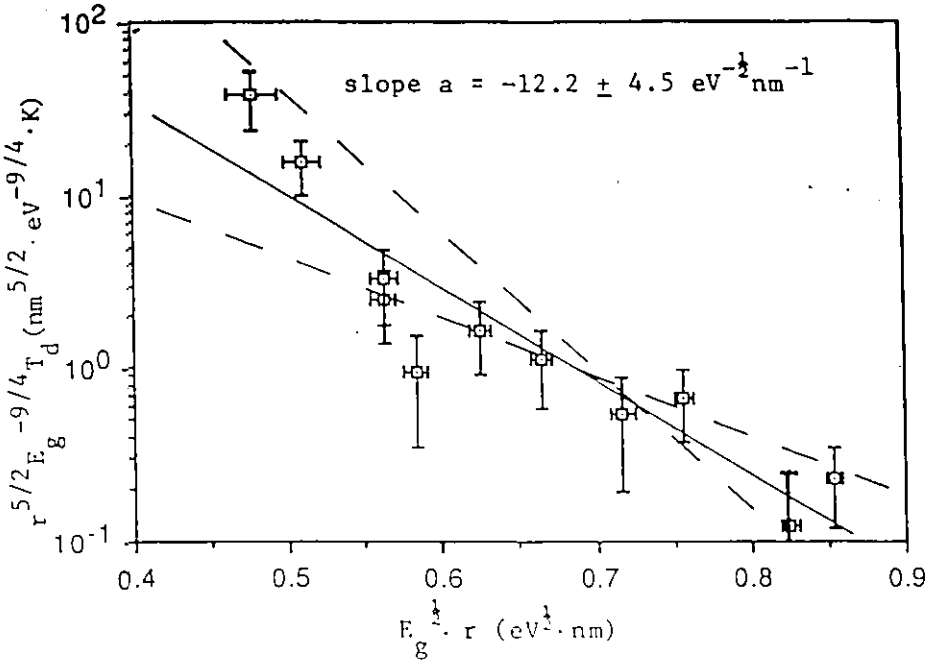

Figure 3.10 Graph of data points analysed according to Abrikosov's equation (equation 3-7)

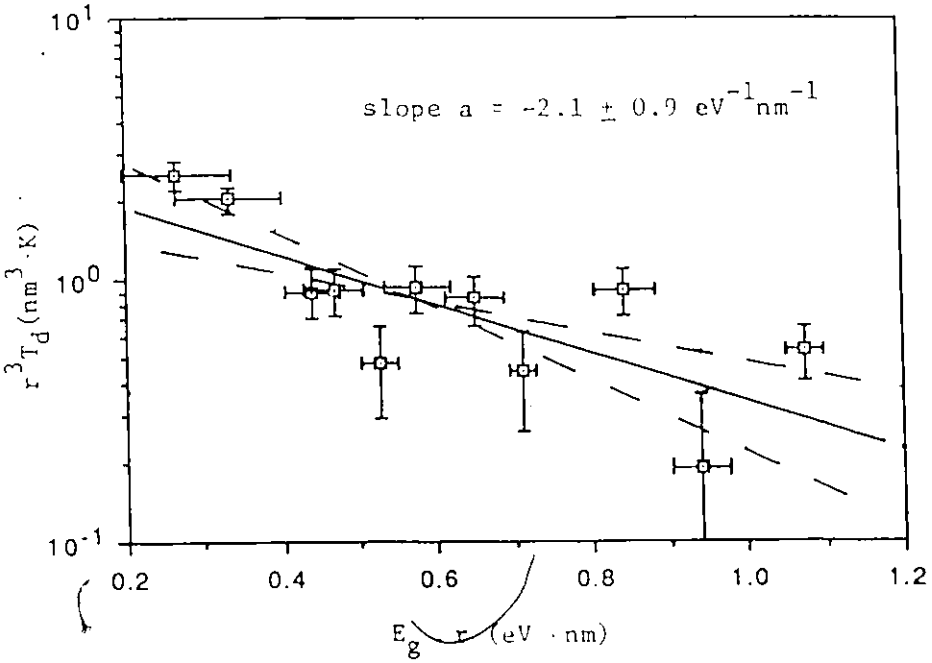

Figure 3.11 Graph of data points analysed according to Bloembergen and Rowland's equation (3-5).

All of the above values were obtained using room temperature energy gaps. Strictly speaking, the analysis should be performed using the energy gap at the spin glass transition temperature. In order to see if the change in energy gap would affect the final result, low temperature values of the energy gaps were calculated. This was done using the composition and temperature dependence of the energy gap for CdHgTe (73M1, p. 396). The change in energy gap used was based on a change in temperature of -300K:

$$\Delta E_g = -0.17\left(\frac{x}{x + y} - 0.5\right) \text{ eV} \qquad (3\text{-}12)$$

New graphs corresponding to equations 3-7 and 3-5 are given in Figures 3.12 and 3.13 respectively. The slopes were calculated to be $a = -12.7 \pm 2.5$ and $a = -2.0 \pm 0.9$ respectively, and thus have negligible difference from those obtained using room temperature energy gaps. Because the temperature dependence of the energy gaps of HgTe and CdTe are almost equal and opposite, it seems the data is merely stretched out, leaving the slopes almost unaffected.

3.5 Discussion and conclusions

The results of the analysis of the magnetic and optical properties of CdHgMnTe indicate a significant enhancement of the exchange interaction when the energy gap becomes small. These results show at least qualitative agreement with the energy gap dependence predicted by Bloembergen and Rowland (55B1) and Abrikosov (80A1). Of the two, the Bloembergen-Rowland theoretical result has better agreement with experimental data than that of Abrikosov. This may be due to

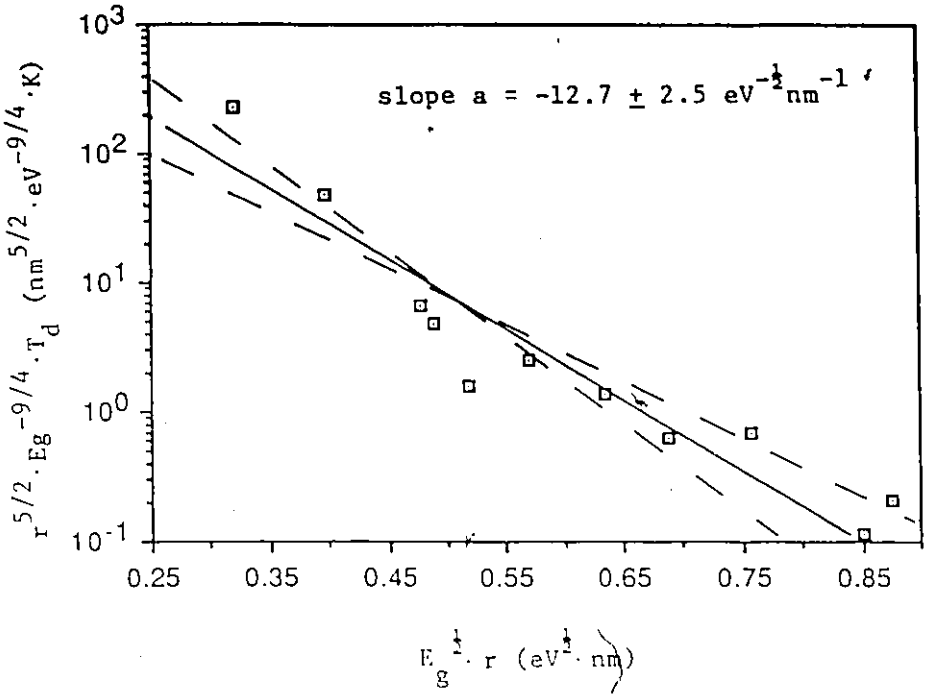

Figure 3.12 Graph of data points as in figure 3.10 for Abrikosov's equation (3-7), but with low temperature energy gap.

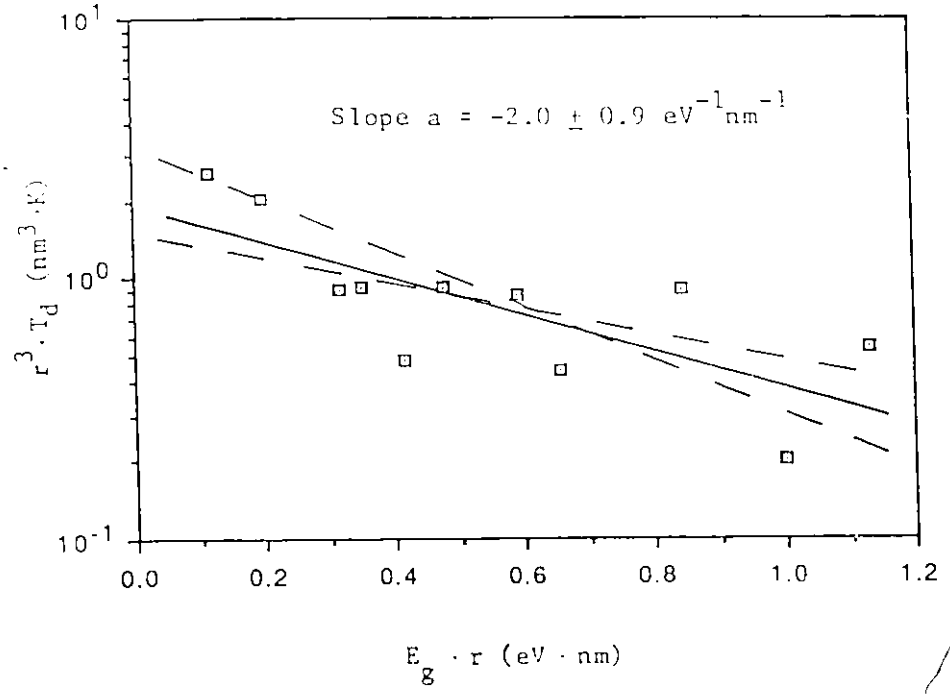

Figure 3.13 Graph of data points as in figure 3.11 for Bloembergen and Rowland's equation (3-5), but with low temperature energy gap.

the stretching of Abrikosov's result to manganese concentrations for which it is not applicable.

However, experimental error prevents the forming of any definitive conclusion on the correctness of either prediction. This error can be attributed to two factors: the uncertainty in composition, especially manganese concentration, in the materials used in the study; and the error in determining the difference in spin glass transition temperature, T_d, due solely to the Bloembergen-Rowland interaction.

The first problem is not evident, as the data seems quite self consistent. However, a systematic change in composition, perhaps by the loss of mercury, could alter the results considerably. A solution to the composition problem might be achieved by actual chemical (or other) measurement of each sample. Another method would be to see if the fabrication techniques could be altered to minimize possible compositional changes (e.g. annealing with extra mercury present).

The second problem, the error on T_d, would be harder to fix. The measurement of the actual transition temperature, T_g, has a small error associated with it, usually less than 0.5 K. However, T_d is also small, being at most 4.3K. Thus a large error must be accepted as unavoidable. However, extending measurements to lower energy gaps and temperatures below 4.2K would provide more data points with high T_d values.

SUMMARY AND GENERAL CONCLUSIONS

4.1 Summary

This thesis deals with the subject of semimagnetic semiconductors. This field has attracted great interest recently, due to the many properties affected by the introduction of a magnetic component to a semiconductor lattice, and to the magnetic behaviour of such a diluted magnetic system.

Specifically, this thesis contributes to two areas of the research into SMSC's. The first of these is the growth of bulk single crystals of the pseudo-ternary alloy $Cd_xZn_yMn_zTe$ $(x + y + z = 1)$ and the comparison of the properties of these single crystals with polycrystals of the same nominal composition.

An abbreviated attempt was also made to grow single crystals of $Cd_xHg_yMn_zTe$ $(x + y + z = 1)$.

The second area of interest which was investigated was the effect of a small energy gap on the magnetic properties of SMSC's. For this study, polycrystalline samples of various compositions of $Cd_xHg_yMn_zTe$ $(x + y + z = 1)$ were made. Powder X-ray, magnetic susceptibility and energy gap measurements were performed, and the results were analysed according to the theoretical work of Bloembergen and Rowland (55Bl) and Abrikosov (80Al).

4.2 Single Crystal Growth

Single crystal specimens of CdZnMnTe were grown by the Bridgman method. Complete single crystals were obtained only when the ingot was annealed for an extra day after growth. This may suggest the need for a slower growth rate than the 5mm/hr used.

Comparison of X-ray and magnetic susceptibility properties showed that the polycrystals and single crystals were the same, within 10% of the nominal composition values. This in turn implies a narrow separation of the solidus and liquidus surfaces of the CdZnMnTe pseudo-ternary phase diagram. However, a comprehensive investigation of the phase diagram would require many more single crystals to be grown, over the complete range of solid solution.

The first attempt at growing another alloy, CdHgMnTe, resulted in a polycrystal with grains larger than 1 mm diameter. A second sample of CdHgMnTe exploded while annealing, destroying the sample holder and damaging the furnace. No attempts were made to compare single crystals with polycrystals for CdHgMnTe, as work on the properties of polycrystalline samples is currently being performed by Mr. S. Manhas for the whole range of compositions, and has not yet been completed.

There is unlimited room for further research into single crystal growth of CdZnMnTe, CdHgMnTe and other SMSC alloys. In addition to the standard Bridgman method, chemical vapour transport also holds promise as a means of growing SMSC single crystals.

4.3 Magnetic Properties of the Narrow Band-gap Alloy $Cd_xHg_yMn_zTe$ $(x + y + z = 1)$

Many alloys of $Cd_xHg_yMn_zTe$ $(x + y + z = 1)$ were made by the melt and anneal technique. The compositions were chosen to allow for a large range of energy gap, so as to study the effect of a small gap on the magnetic properties. The magnetic properties of the alloys with narrow gaps were expected to differ from those with wide gaps, due to an extra exchange mechanism resulting from virtual transitions across the gap.

The exchange energy was measured by determining the position of a cusp in the magnetic susceptibility-temperature graphs. This cusp is believed to be due to a change from a spin glass to a paramagnetic state when the thermal energy kT becomes greater than the exchange energy.

X-ray, magnetic and optical measurements were performed on the CdHgMnTe samples. Interpolations of the exchange energy for hypothetical wide gap samples of identical structure (zinc blende) were made using the experimental results from other alloy systems with zinc blende structure but wide gaps.

The enhancement of the exchange energy in the narrow gap samples was found to be significant. The spin glass transition temperature was found to increase by as much as 4.3 ± 0.5 K above that of the corresponding wide gap temperature.

Analysis of the experimental data was performed using theoretical relations for the exchange energy found in the literature (55Bl, 80Al). The results agreed more with Bloembergen and Rowland than

with Abrikosov. This was unexpected as Abrikosov's derivation dealt specifically with semiconductor spin glasses and pointed out errors in Bloembergen's and Rowland's methods. Also, Bloembergen and Rowland were studying nuclear spin exchange in thallium and thallic oxide. Abrikosov's derivation, though, was based on low concentrations of the magnetic component and may have been extended past its applicable range. However, the experimental errors were large enough to rule out complete rejection or acceptance of either theoretical prediction.

These results thus leave ample room for further research into the exchange interaction in narrow gap SMSC's. In addition to improving the analysis of CdHgMnTe, other narrow gap alloy systems should be investigated. Suggested alloys are HgMnSe and PbSnMnTe, both of which have low energy gaps and fairly wide ranges of solid solution.

REFERENCES

25B1 Bridgman, P.W., 1925, Proc. Amer. Acad. Arts Sci., 60, 305.

55B1 Bloembergen, N., and Rowland T.J., 1955, Phys. Rev., 97, 1679.

60W1 Woolley, J.C., and Ray, B., 1960, J. Phys. Chem. Solids, 13, 151.

63D1 Delves, R.T., and Lewis, B., 1963, J. Phys. Chem. Solids, 24, 549.

70L1 Long, D., and Schmit, J.L., 1970, Semiconductors and Semimetals, Vol. 5, edited by Willardson, R.K., and Beer, A.C., Academic Press, New York and London.

72B1 Basinski, J., 1972, Doctoral Thesis, University of Ottawa.

72S1 Steininger, J., and Strauss, A., 1972, J. Crystal Growth, 13/14, 657.

73B1 Brice, J.C., 1973, the Growth of Crystals From Liquids, North-Holland, Amsterdam.

73M1 Moss, T.S., Burrell, G.J., and Ellis, B., 1973, Semiconductor Opto-Electronics, John Wiley and Sons, New York.

77G1 Geertsma, W., Haas, C., Sawatzky, G.A., and Vertogen, G., 1977, Physica B, 86-88, 1039.

78C1 Cullity, B.D., 1978, Elements of X-ray Diffraction, 2nd ed., Addison-Wesley, Reading.

79B1 Bastard, G., and Lewiner, C., 1979, Phys. Rev. B, 20, 4256.

80A1 Abrikosov, A.A., 1980, Adv. Phys., 29, 869.

80L1 Lewiner, C., Gaj, J.A., and Bastard, G., 1980, J. de Physique, 41, C5-289.

81D1 Debska, U., Dietl, M., Grabacki, G., Janik, E., Kierzek-Pecold, E., and Klimkiewicz, M., 1981, Phys. Stat. Sol. (a), 64, 707.

81E1 Escorne, M., Mauger, A., Triboulet, R., and Tholence, J.L., 1981, Physica B, 107, 309.

81G1 Giebultowicz, T., Kepa, H., Buras, B., Clausen, K., and Galazka, R.R., 1981, Solid St. Commun., 40, 499.

81T1 Triboulet, R., and Didier, G., 1981, J. Crystal Growth, 52, 614.

82G1 Galazka, R.R., 1982, Lect. Notes Phys., 152, 294.

82G2 Goodchild, R.G., Hughes, O.H., Lopez-Rivera, S.A., and Woolley, J.C., 1982, Can. J. Phys., 60, 1096.

82H1 Holden, T.M., Dolling, G., Sears, V.F., Furdyna, J.K., and Giriat, W., 1982, J. Appl. Phys., 53, 1882.

83B1 Brun del Re, R., Donofrio, T., Avon, J., Majid, J., and Woolley, J.C., 1983, Il Nuovo Cimento, 2, 1911.

84B1 Brandt, N.B., and Moschalkov, V.V., 1984, Adv. Phys., 33, 193.

84M1 Mycielski, A., Rigaux, C., Menant, M., Dietl, T., and Otto, M., 1984, Solid St. Commun, 50, 257.

85D1 Donofrio, T., Lamarche, G., and Woolley, J.C., 1985, J. Appl. Phys., 57, 1937.

85L1 Larson, B.E., Hass, K.C., Ehrenreich, H., and Carlsson, A.E., Solid St. Commun., 56, 347.

86S1 Spalek, J., Lewicki, A., Tarnawski, Z., Furdyna, J.K., Galazka, R.R., and Obuszko, Z., 1986, Phys. Rev. B, 33, 3407.

86W1 Woolley, J.C., Donofrio, T., Chehab, S., Manhas, S., Lamarche, G., and Manoogian, A., 1986, J. Magn. Magn. Mat., in press.